

A New Approach of High Order Well-Balanced Finite Volume WENO Schemes and Discontinuous Galerkin Methods for a Class of Hyperbolic Systems with Source Terms[†]

Yulong Xing¹ and Chi-Wang Shu^{2,*}

¹ *Department of Mathematics, Brown University, Providence, RI 02912, USA.*

² *Division of Applied Mathematics, Brown University, Providence, RI 02912, USA.*

Received 6 August 2005; Accepted (in revised version) 22 September 2005

Abstract. Hyperbolic balance laws have steady state solutions in which the flux gradients are nonzero but are exactly balanced by the source terms. In our earlier work [31–33], we designed high order well-balanced schemes to a class of hyperbolic systems with separable source terms. In this paper, we present a different approach to the same purpose: designing high order well-balanced finite volume weighted essentially non-oscillatory (WENO) schemes and Runge-Kutta discontinuous Galerkin (RKDG) finite element methods. We make the observation that the traditional RKDG methods are capable of maintaining certain steady states exactly, if a small modification on either the initial condition or the flux is provided. The computational cost to obtain such a well balanced RKDG method is basically the same as the traditional RKDG method. The same idea can be applied to the finite volume WENO schemes. We will first describe the algorithms and prove the well balanced property for the shallow water equations, and then show that the result can be generalized to a class of other balance laws. We perform extensive one and two dimensional simulations to verify the properties of these schemes such as the exact preservation of the balance laws for certain steady state solutions, the non-oscillatory property for general solutions with discontinuities, and the genuine high order accuracy in smooth regions.

Key words: Hyperbolic balance laws; WENO finite volume scheme; discontinuous Galerkin method; high order accuracy; source term; conservation laws; shallow water equation; elastic wave equation; chemosensitive movement; nozzle flow; two phase flow.

*Correspondence to: Chi-Wang Shu, Division of Applied Mathematics, Brown University, Providence, RI 02912, USA. E-mail: shu@dam.brown.edu

[†]Research supported by ARO grant W911NF-04-1-0291, NSF grant DMS-0510345 and AFOSR grant FA9550-05-1-0123.

1 Introduction

In this paper, we are concerned with the construction of high order well balanced weighted essentially non-oscillatory (WENO) finite volume schemes and Runge-Kutta discontinuous Galerkin (RKDG) finite element methods for solving hyperbolic balance laws, which have attracted significant attention in the past few years. Hyperbolic balance laws are hyperbolic systems of conservation laws with source terms:

$$u_t + f_1(u, x, y)_x + f_2(u, x, y)_y = g(u, x, y) \quad (1.1)$$

or in the one dimensional case

$$u_t + f(u, x)_x = g(u, x) \quad (1.2)$$

where u is the solution vector, $f_1(u, x, y)$ and $f_2(u, x, y)$ (or $f(u, x)$) are the fluxes and $g(u, x, y)$ (or $g(u, x)$) is the source term.

An essential part for these balance laws is that they often admit steady state solutions in which the flux gradients are exactly balanced by the source term. A straightforward treatment of the source terms in a numerical scheme will fail to preserve this balance. Many physical phenomena come from small perturbations of these steady state solutions, which are very difficult to capture numerically, unless the numerical schemes can preserve the unperturbed steady state at the discrete level. Schemes which can preserve the unperturbed steady state at the discrete level are the so called well balanced schemes. Our purpose is to design well balanced schemes without sacrificing the high order accuracy and non-oscillatory properties of the scheme when applied to general, non-steady state solutions.

Balance laws have many applications in the physical world. A typical and extensively considered example is the shallow water equations with a non flat bottom topology. Many geophysical flows are modeled by the variants of the shallow water equations. In one space dimension, they take the form

$$\begin{cases} h_t + (hu)_x = 0 \\ (hu)_t + \left(hu^2 + \frac{1}{2}gh^2\right)_x = -ghb_x, \end{cases} \quad (1.3)$$

where h denotes the water height, u is the velocity of the fluid, b represents the bottom topography and g is the gravitational constant. The steady state solutions are given by

$$hu = constant \quad and \quad \frac{1}{2}u^2 + g(h + b) = constant. \quad (1.4)$$

People are particularly interested in the still water stationary solution, denoted by

$$u = 0 \quad and \quad h + b = constant. \quad (1.5)$$

Bermudez and Vazquez [4] first introduced the concept of the “exact C-property”, which means that the scheme is “exact” when applied to the still water stationary solution (1.5). Also, they introduced the first order Q-scheme and the idea of source term upwinding to obtain such

property. After this, many well balanced schemes for the shallow water equations have been developed in the literature, mostly for first and second order accuracy, e.g. [2,17–19,22,28–30,34].

In our recent work [31–33], we have successfully developed high order well balanced finite difference, finite volume WENO schemes and RKDG methods for a class of hyperbolic balanced laws with separable source terms. This class of hyperbolic systems includes the shallow water equations mentioned above, the elastic wave equation, the hyperbolic model for a chemosensitive movement, the nozzle flow, a model from fluid mechanics and a two phase flow model. In [31], we developed a well balanced high order finite difference WENO scheme for solving the shallow water equations, which is non-oscillatory, well balanced (satisfying the exact C-property) for still water, and genuinely high order in smooth regions. In [32], we extended the process to a general class of balance laws with separable source terms, allowing the design of well balanced high order finite difference WENO scheme for all balance laws falling into this category. In [33], well balanced high order finite volume WENO schemes and finite element discontinuous Galerkin schemes on general triangulations were designed for the same class of balance laws as those in [32], which are more suitable for computations in complex geometry and / or for using adaptive meshes. The key ingredient of the technique used in [31–33] to obtain well balanced property is a special decomposition of the source term, allowing a discretization to the source term to be both high order accurate for general solutions and exactly well balanced with the flux gradient for some steady states.

In this paper, we consider RKDG methods first, and show that the traditional RKDG methods can achieve the well balanced property with a small modification of either the initial value or the flux. This is by far the simplest approach to obtain a high order well balanced scheme. Very little additional computational cost over the traditional RKDG methods is involved to obtain a well balanced property. Similar ideas are then applied to obtain well balanced finite volume WENO schemes. We emphasize that the setup in this paper for well balanced schemes is completely different from the one used in our previous paper [33], rather it is a generalization of a well-balanced high order scheme recently developed by Noelle et al. [21], see Remark 4.3 in Section 4. Comparing with the schemes in our previous work [33], the schemes presented here require less computational cost, and are easier to understand and to code, at least for the RKDG methods. For the cases we have tested, this simpler approach seems to yield comparably good numerical results. We will first describe the algorithms and prove the well balanced property for the shallow water equations, and then generalize the result to a class of other balance laws.

The paper is organized as follows. In Section 2, we give a brief review of finite volume WENO schemes and RKDG schemes. In Section 3, we develop genuine high order well-balanced RKDG schemes for the shallow water equations. The well-balanced generalization of finite volume WENO schemes is presented in Section 4. Section 5 contains extensive numerical simulation results to demonstrate the behavior of our well balanced schemes for one and two dimensional shallow water equations, verifying high order accuracy, the exact C-property, and good resolution for smooth and discontinuous solutions. Application of these ideas to other balance laws, together with some selective numerical tests, are presented in Section 6. In Section 7, we give the concluding remarks.

2 A review of high order finite volume WENO and discontinuous Galerkin schemes

In this section, we briefly review the basic ideas of finite volume WENO schemes and discontinuous Galerkin methods. For further details about these subjects, we refer to [3, 5–10, 15, 16, 20, 23, 25–27].

We consider a scalar hyperbolic conservation law equation in one dimension

$$u_t + f(u)_x = 0, \quad (2.1)$$

and discretize the computational domain with cells $I_i = [x_{i-\frac{1}{2}}, x_{i+\frac{1}{2}}]$, $i = 1, \dots, N$. We denote the size of the i -th cell by Δx_i and the center of the cell by $x_i = \frac{1}{2}(x_{i-\frac{1}{2}} + x_{i+\frac{1}{2}})$.

In a finite volume scheme, our computational variables are $\bar{u}_i(t)$, which approximate the cell averages $\bar{u}(x_i, t) = \frac{1}{\Delta x_i} \int_{I_i} u(x, t) dx$. The conservative numerical scheme is given by:

$$\frac{d}{dt} \bar{u}_i(t) = -\frac{1}{\Delta x_i} \left(\hat{f}_{i+\frac{1}{2}} - \hat{f}_{i-\frac{1}{2}} \right) \quad (2.2)$$

with $\hat{f}_{i+\frac{1}{2}} = F(u_{i+\frac{1}{2}}^-, u_{i+\frac{1}{2}}^+)$ being the numerical flux. Here $u_{i+\frac{1}{2}}^-$ and $u_{i+\frac{1}{2}}^+$ are the high order pointwise approximations to $u(x_{i+\frac{1}{2}}, t)$, obtained from the cell averages by a high order WENO reconstruction procedure. The numerical flux $F(a, b)$ needs to be monotone. The simplest and most inexpensive monotone flux is the Lax-Friedrichs flux:

$$F(a, b) = \frac{1}{2}(f(a) + f(b) - \alpha(b - a)), \quad (2.3)$$

where $\alpha = \max_u |f'(u)|$.

The approximations $u_{i+\frac{1}{2}}^-$ and $u_{i+\frac{1}{2}}^+$ are computed through the neighboring cell average values \bar{u}_j . Basically, for a $(2k-1)$ -th order WENO scheme, we first compute k reconstructed boundary values $u_{i+\frac{1}{2}}^{(k),\pm}$ corresponding to different candidate stencils. Then by providing each value a weight which indicates the smoothness of the corresponding stencil, we define the $(2k-1)$ -th order WENO reconstruction $u_{i+\frac{1}{2}}^\pm$ as a convex combination of all these k reconstructed values. The complete algorithm can be found in [16, 23, 25].

For hyperbolic systems, we usually use the local characteristic decomposition, which is more robust than a component by component version. Together with a TVD high order Runge-Kutta time discretization [26], this completes the description of a high order finite volume WENO scheme.

Finite volume WENO schemes in the two dimensional case have the same framework but are more complicated to implement. In this paper, we consider only rectangular cells for simplicity. For the two dimensional homogeneous conservation law

$$u_t + f_1(u, x, y)_x + f_2(u, x, y)_y = 0, \quad (2.4)$$

together with a spatial discretization of the computational domain by cells $I_{ij} = [x_{i-\frac{1}{2}}, x_{i+\frac{1}{2}}] \times [y_{j-\frac{1}{2}}, y_{j+\frac{1}{2}}]$, $i = 1, \dots, N_x$, $j = 1, \dots, N_y$, we use the notations as usual:

$$\Delta x_i = x_{i+\frac{1}{2}} - x_{i-\frac{1}{2}}, \quad \Delta y_j = y_{j+\frac{1}{2}} - y_{j-\frac{1}{2}}$$

to denote the grid sizes.

By taking the integral of the equation, we can obtain the conservative scheme

$$\frac{d}{dt} \bar{u}_{ij}(t) = -\frac{1}{\Delta x_i} \left((\hat{f}_1)_{i+\frac{1}{2},j} - (\hat{f}_1)_{i-\frac{1}{2},j} \right) - \frac{1}{\Delta y_j} \left((\hat{f}_2)_{i,j+\frac{1}{2}} - (\hat{f}_2)_{i,j-\frac{1}{2}} \right), \quad (2.5)$$

where the numerical flux $(\hat{f}_1)_{i+\frac{1}{2},j}$ is defined by

$$(\hat{f}_1)_{i+\frac{1}{2},j} = \sum_{\alpha} w_{\alpha} F \left(u_{x_{i+\frac{1}{2}},y_j+\beta_{\alpha}\Delta y_j}^{-}, u_{x_{i+\frac{1}{2}},y_j+\beta_{\alpha}\Delta y_j}^{+} \right) \quad (2.6)$$

where β_{α} and w_{α} are the Gaussian quadrature nodes and weights, to approximate the integration in y :

$$\frac{1}{\Delta y_j} \int_{y_{j-\frac{1}{2}}}^{y_{j+\frac{1}{2}}} f_1(u(x_{i+\frac{1}{2}}, y, t)) dy.$$

The monotone flux $F(a, b)$ is the same as above (for example, Formula (2.3)). $u_{x_{i+\frac{1}{2}},y_j+\beta_{\alpha}\Delta y_j}^{\pm}$ are the $(2k - 1)$ -th order accurate reconstructed values obtained by a WENO reconstruction procedure. Similarly, we can compute the flux $(\hat{f}_2)_{i,j+\frac{1}{2}}$.

In a high order RKDG scheme, we seek an approximation u_h to u which belongs to the finite dimensional space

$$V_h = V_h^k \equiv \{v : v|_{I_j} \in P^k(I_j), j = 1, \dots, N\}, \quad (2.7)$$

where $P^k(I)$ denotes the space of polynomials in I of degree at most k . The numerical scheme is given by

$$\int_{I_j} \partial_t u_h(x, t) v_h(x) dx - \int_{I_j} f(u_h(x, t)) \partial_x v_h(x) dx + \hat{f}_{j+\frac{1}{2}} v_h(x_{j+\frac{1}{2}}^{-}) - \hat{f}_{j-\frac{1}{2}} v_h(x_{j-\frac{1}{2}}^{+}) = 0, \quad (2.8)$$

As before, $\hat{f}_{j+\frac{1}{2}} = F(u_h(x_{j+\frac{1}{2}}^{-}, t), u_h(x_{j+\frac{1}{2}}^{+}, t))$, and $F(a, b)$ is chosen as a monotone flux. We could, for example, again use the simple Lax-Friedrichs flux (2.3).

Another important ingredient for the RKDG method is that a slope limiter procedure might be needed after each inner stage in the Runge-Kutta time stepping, when the solution contains discontinuities. In this paper we use the total variation bounded (TVB) limiter in [6, 8, 9, 24]; we refer to these references for the details of this limiter.

Together with a TVD high order Runge-Kutta time discretization [26], we have then finished the description of the RKDG method.

Multi-dimensional problems can be handled in the same fashion. The main difference is that the fluxes are now integrals along the cell boundary, which can be calculated by Gauss-quadrature rules.

3 Construction of well balanced RKDG schemes for shallow water equations

The traditional high order RKDG method has been presented in Section 2. In this section, we claim that, for one-dimensional and two-dimensional shallow water equations, this method is indeed a well balanced scheme for still water, based on a suitable choice of the initial value or the flux. This choice will not affect the property of the scheme, such as high order accuracy in smooth region and non-oscillatory shock resolution, and it increases the computational cost only slightly.

For the shallow water equations (1.3), we are interested in preserving the still water stationary solution (1.5). For this still water, the first equation $(hu)_x = 0$ is satisfied exactly for any consistent scheme since $hu = 0$. Let us concentrate on the second equation, which can be denoted by

$$(hu)_t + f(U)_x = g(h, b)$$

where $U = (h, hu)^T$ with the superscript T denoting the transpose.

As described in Section 3, in a RKDG method U is approximated by the piecewise polynomial U_h , which belongs to V_h defined in (2.7). We project the bottom function b into the same space V_h , to obtain an approximation b_h . This implies that $h_h + b_h = \text{constant}$ if $h + b = \text{constant}$.

Following the idea first introduced by Audusse et al. [1], and later used in the recent paper by Noelle et al. [21], our numerical scheme has the form:

$$\int_{I_j} \partial_t (hu)_h v_h dx - \int_{I_j} f(U_h) \partial_x v_h dx + \hat{f}_{j+\frac{1}{2}}^l v_h(x_{j+\frac{1}{2}}^-) - \hat{f}_{j-\frac{1}{2}}^r v_h(x_{j-\frac{1}{2}}^+) = \int_{I_j} g(h_h, b_h) v_h dx. \quad (3.1)$$

Comparing with the standard RKDG scheme (2.8), we can see that the single valued fluxes $\hat{f}_{j+\frac{1}{2}}$ and $\hat{f}_{j-\frac{1}{2}}$ have been replaced by the left flux $\hat{f}_{j+\frac{1}{2}}^l$ and the right flux $\hat{f}_{j-\frac{1}{2}}^r$, respectively. We can rewrite the above scheme as:

$$\begin{aligned} \int_{I_j} \partial_t (hu)_h v_h dx - \int_{I_j} f(U_h) \partial_x v_h dx + \hat{f}_{j+\frac{1}{2}}^l v_h(x_{j+\frac{1}{2}}^-) - \hat{f}_{j-\frac{1}{2}}^r v_h(x_{j-\frac{1}{2}}^+) = & \quad (3.2) \\ \int_{I_j} g(h_h, b_h) v_h dx + (\hat{f}_{j+\frac{1}{2}} - \hat{f}_{j+\frac{1}{2}}^l) v_h(x_{j+\frac{1}{2}}^-) - (\hat{f}_{j-\frac{1}{2}} - \hat{f}_{j-\frac{1}{2}}^r) v_h(x_{j-\frac{1}{2}}^+), \end{aligned}$$

where $\hat{f}_{j+\frac{1}{2}} = F(U_h(x_{j+\frac{1}{2}}^-, t), U_h(x_{j+\frac{1}{2}}^+, t))$. The left side of (3.2) is the traditional RKDG scheme, and the right side is our approximation to the source term. The design of the left flux $\hat{f}_{j+\frac{1}{2}}^l$ and the right flux $\hat{f}_{j-\frac{1}{2}}^r$ will be explained later, however we point out here that $\hat{f}_{j+\frac{1}{2}} - \hat{f}_{j+\frac{1}{2}}^l$ and $\hat{f}_{j-\frac{1}{2}} - \hat{f}_{j-\frac{1}{2}}^r$ are high order correction terms at the level of $O(\Delta x^{k+1})$. Therefore, the scheme (3.1) is a $(k+1)$ -th order conservative scheme and will converge to the weak solution.

In order to obtain the well balanced property, we need the residue

$$R = - \int_{I_j} f(U_h) \partial_x v_h dx + \hat{f}_{j+\frac{1}{2}}^l v_h(x_{j+\frac{1}{2}}^-) - \hat{f}_{j-\frac{1}{2}}^r v_h(x_{j-\frac{1}{2}}^+) - \int_{I_j} g(h_h, b_h) v_h dx \quad (3.3)$$

to be zero if the still water stationary state (1.5) is reached. The following three conditions, which only need to be valid for the still water stationary state, are sufficient to guarantee this zero residue property.

- All the integrals in formula (3.3) should be calculated exactly for the still water. This can be easily achieved by using suitable Gauss-quadrature rules since h_h, b_h and v_h are polynomials in each cell I_j , hence f, g are both polynomials. Note that $(hu)_h = 0$ for the still water.
- We assume that

$$\hat{f}_{j+\frac{1}{2}}^l = f(U_h(x_{j+\frac{1}{2}}^-, t)), \quad \hat{f}_{j-\frac{1}{2}}^r = f(U_h(x_{j-\frac{1}{2}}^+, t)) \tag{3.4}$$

for the still water. Note that this condition is not obvious. Later we will comment on how to make it possible for the RKDG method.

- We assume that U_h , which is the numerical approximation of U , is a steady state solution of the equation $(hu)_t + f(U)_x = g(h, b_h)$, where b_h has substituted b . This is true since $h_h + b_h = \text{constant}$ and $(hu)_h = 0$, which imply $(\frac{1}{2}gh_h^2)_x = -gh_h(b_h)_x$, or

$$\partial_x f(U_h) = g(h_h, b_h). \tag{3.5}$$

Proposition 3.1: RKDG schemes which satisfy the above three conditions for the shallow water equations are exact for the still water stationary state (1.5).

Proof: If these three conditions are satisfied, the residue R in (3.3) for still water reduces to

$$\begin{aligned} R &= - \int_{I_j} f(U_h) \partial_x v_h dx + \hat{f}_{j+\frac{1}{2}}^l v_h(x_{j+\frac{1}{2}}^-) - \hat{f}_{j-\frac{1}{2}}^r v_h(x_{j-\frac{1}{2}}^+) - \int_{I_j} g(h_h, b_h) v_h dx \\ &= - \int_{I_j} f(U_h) \partial_x v_h dx + f(U_h(x_{j+\frac{1}{2}}^-, t)) v_h(x_{j+\frac{1}{2}}^-) - f(U_h(x_{j-\frac{1}{2}}^+, t)) v_h(x_{j-\frac{1}{2}}^+) - \int_{I_j} g(h_h, b_h) v_h dx \\ &= \int_{I_j} \partial_x f(U_h) v_h dx - \int_{I_j} g(h_h, b_h) v_h dx \\ &= \int_{I_j} (\partial_x f(U_h) - g(h_h, b_h)) v_h dx = 0 \end{aligned}$$

where the second equality is due to (3.4), the third equality follows from a simple integration by parts, and the last equality follows from (3.5). ■

Remark 3.2: For discontinuous solutions, the limiter on the function U_h is usually performed after each Runge-Kutta stage. This limiter procedure might destroy the preservation of the still water steady state $h + b = \text{constant}$. Therefore, following the idea presented in [1, 34], we apply the limiter procedure on the function $(h_h + b_h, (hu)_h)^T$ instead. The modified RKDG solution is then defined by $h_h^{mod} \equiv (h + b)_h^{mod} - b_h$. Since $\overline{h_h^{mod}} = \overline{(h + b)_h^{mod}} - \overline{b_h} = \overline{(h + b)_h} - \overline{b_h} = \overline{h_h}$, we

observe that this procedure will not destroy the conservativity of h_h , which should be maintained during the limiter process. ■

For shallow water equations, the first and third conditions are obviously true, hence the only one remaining for us to check is the second condition. In order to fulfill it, we have two choices.

Choice A: Define the initial value and the approximation b_h by continuous piecewise polynomials. We would then have $b_h(x_{j+\frac{1}{2}}^-, t) = b_h(x_{j+\frac{1}{2}}^+, t)$. If the steady state $h_h + b_h = \text{constant}$ is reached, we will have a continuous h_h , i.e. $h_h(x_{j+\frac{1}{2}}^-, t) = h_h(x_{j+\frac{1}{2}}^+, t)$, which makes

$$\hat{f}_{j+\frac{1}{2}} = F(U_h(x_{j+\frac{1}{2}}^-, t), U_h(x_{j+\frac{1}{2}}^+, t)) = f(U_h(x_{j+\frac{1}{2}}^-, t)) = f(U_h(x_{j+\frac{1}{2}}^+, t))$$

We can therefore simply define the left and right fluxes as

$$\hat{f}_{j+\frac{1}{2}}^l = \hat{f}_{j+\frac{1}{2}}, \quad \hat{f}_{j-\frac{1}{2}}^r = \hat{f}_{j-\frac{1}{2}},$$

which will fulfill the second condition. This make our scheme (3.1) to be identical to the traditional RKDG scheme without any modification.

In order to define the continuous piecewise polynomial approximations to the initial value and b , we can use the idea of essentially non-oscillatory (ENO) procedure [13]. Based on the values $u_{j+\frac{1}{2}}$, we can choose suitable stencils for each individual cell I_j by an ENO procedure, and then obtain a polynomial on I_j through an interpolation. This polynomial equals to $u_{j-\frac{1}{2}}$ and $u_{j+\frac{1}{2}}$ at the two cell boundaries. Hence the global piecewise polynomial is continuous.

Choice B: Here we follow the idea of Audusse et al. [1]. After computing boundary values $U_{h,j+\frac{1}{2}}^\pm$, we set

$$h_{h,j+\frac{1}{2}}^{*,+} = \max \left(0, h_{h,j+\frac{1}{2}}^+ + b_{h,j+\frac{1}{2}}^+ - \max(b_{h,j+\frac{1}{2}}^+, b_{h,j+\frac{1}{2}}^-) \right) \tag{3.6}$$

$$h_{h,j+\frac{1}{2}}^{*,-} = \max \left(0, h_{h,j+\frac{1}{2}}^- + b_{h,j+\frac{1}{2}}^- - \max(b_{h,j+\frac{1}{2}}^+, b_{h,j+\frac{1}{2}}^-) \right) \tag{3.7}$$

and redefine the left and right values of U as:

$$U_{h,j+\frac{1}{2}}^{*,\pm} = \begin{pmatrix} h_{h,j+\frac{1}{2}}^{*,\pm} \\ (hu)_{h,j+\frac{1}{2}}^\pm \end{pmatrix} \tag{3.8}$$

Then the left and right fluxes $\hat{f}_{j+\frac{1}{2}}^l$ and $\hat{f}_{j-\frac{1}{2}}^r$ are given by:

$$\hat{f}_{j+\frac{1}{2}}^l = F(U_{h,j+\frac{1}{2}}^{*,-}, U_{h,j+\frac{1}{2}}^{*,+}) + \begin{pmatrix} 0 \\ \frac{g}{2}(h_{h,j+\frac{1}{2}}^-)^2 - \frac{g}{2}(h_{h,j+\frac{1}{2}}^{*,-})^2 \end{pmatrix} \tag{3.9}$$

$$\hat{f}_{j-\frac{1}{2}}^r = F(U_{h,j-\frac{1}{2}}^{*, -}, U_{h,j-\frac{1}{2}}^{*, +}) + \begin{pmatrix} 0 \\ \frac{g}{2}(h_{h,j-\frac{1}{2}}^+)^2 - \frac{g}{2}(h_{h,j-\frac{1}{2}}^{*, +})^2 \end{pmatrix} \quad (3.10)$$

Here F is a monotone flux as mentioned in Section 2. It is easy to check that $\hat{f}_{j+\frac{1}{2}}^l - \hat{f}_{j+\frac{1}{2}}^l$ and $\hat{f}_{j-\frac{1}{2}}^l - \hat{f}_{j-\frac{1}{2}}^r$ are indeed at the level of $O(\Delta x^{k+1})$ for general solutions, hence the original $(k+1)$ -th order of accuracy is maintained. Under the still water stationary state, $h_h + b_h = constant$, hence it is easy to see $U_{h,j+\frac{1}{2}}^{*, -} = U_{h,j+\frac{1}{2}}^{*, +}$. The left flux then returns to:

$$\hat{f}_{j+\frac{1}{2}}^l = \begin{pmatrix} 0 \\ \frac{g}{2}(h_{h,j+\frac{1}{2}}^{*, -})^2 \end{pmatrix} + \begin{pmatrix} 0 \\ \frac{g}{2}(h_{h,j+\frac{1}{2}}^-)^2 - \frac{g}{2}(h_{h,j+\frac{1}{2}}^{*, -})^2 \end{pmatrix} = \begin{pmatrix} 0 \\ \frac{g}{2}(h_{h,j+\frac{1}{2}}^-)^2 \end{pmatrix} = f(U_{h,j+\frac{1}{2}}^-) \quad (3.11)$$

Similarly,

$$\hat{f}_{j+\frac{1}{2}}^r = f(U_{h,j+\frac{1}{2}}^+). \quad (3.12)$$

Remark 3.3: Clearly Choice A provides a simpler scheme with smaller computational cost, hence it would be preferred if it provides comparable numerical results to that of Choice B. Unfortunately, although it works well for small perturbation solutions from still water for a smooth bottom, the numerical resolution for a discontinuous bottom is not ideal. On the other hand, Choice B provides good numerical results for all the test cases we have experimented. In Section 5, we will report only the results obtained by Choice B to save space. ■

We now consider the extension of the well-balanced high order RKDG schemes to 2-D shallow water equations

$$\begin{cases} h_t + (hu)_x + (hv)_y = 0 \\ (hu)_t + \left(hu^2 + \frac{1}{2}gh^2\right)_x + (huv)_y = -ghb_x \\ (hv)_t + (huv)_x + \left(hv^2 + \frac{1}{2}gh^2\right)_y = -ghb_y \end{cases} \quad (3.13)$$

where again h is the water height, (u, v) is the velocity of the fluid, b represents the bottom topography and g is the gravitational constant. The still water stationary solution we are interested to preserve is

$$h + b = constant, \quad hu = 0, \quad hv = 0. \quad (3.14)$$

It is straightforward to extend our well balanced RKDG schemes to this two-dimensional problem. Also, the scheme can be applied on any triangulation.

4 Construction of well balanced finite volume WENO schemes for shallow water equations

In this section, we generalize the idea used in Section 3 to design a well balanced finite volume WENO schemes for the shallow water equations. The basic idea is the same as that for the

RKDG methods. The only extra step is due to the fact that we only have the reconstructed pointwise values $U_{j+\frac{1}{2}}^\pm$ and would need to first define an approximation function U_h . We can then follow the procedure as before.

As before, we denote $U_{j+\frac{1}{2}}^\pm$ as the reconstructed left and right values at the interface $x_{j+\frac{1}{2}}$. The still water is given by $\bar{h}_j + \bar{b}_j = \text{constant}$ where as before the overbar denotes the cell average. We would like to have the reconstructed values to satisfy $h_{j+\frac{1}{2}} + b_{j+\frac{1}{2}} = \text{constant}$ as well. This can be achieved by the approach that we used in [33]. Basically, the WENO reconstruction can be eventually written out as

$$U_{j+\frac{1}{2}}^+ = \sum_{k=-r+1}^r w_k \bar{U}_{j+k}, \quad U_{j+\frac{1}{2}}^- = \sum_{k=-r}^{r-1} \tilde{w}_k \bar{U}_{j+k}. \tag{4.1}$$

where $r = 3$ for the fifth order WENO approximation and the coefficients w_k and \tilde{w}_k depend nonlinearly on the smoothness indicators involving the cell average \bar{u} and satisfy $\sum_{k=-r+1}^r w_k = \sum_{k=-r}^{r-1} \tilde{w}_k = 1$. We then use the same coefficients w_k and \tilde{w}_k computed from above on $B = (b, 0)^T$ to obtain

$$B_{j+\frac{1}{2}}^+ = \sum_{k=-r+1}^r w_k \bar{B}_{j+k}, \quad B_{j+\frac{1}{2}}^- = \sum_{k=-r}^{r-1} \tilde{w}_k \bar{B}_{j+k}. \tag{4.2}$$

Hence,

$$U_{j+\frac{1}{2}}^+ + B_{j+\frac{1}{2}}^+ = \sum_{k=-r+1}^r w_k (\bar{U}_{j+k} + \bar{B}_{j+k}), \quad U_{j+\frac{1}{2}}^- + B_{j+\frac{1}{2}}^- = \sum_{k=-r}^{r-1} \tilde{w}_k (\bar{U}_{j+k} + \bar{B}_{j+k}),$$

from which we know that the reconstructed values satisfy $h_{j+\frac{1}{2}}^\pm + b_{j+\frac{1}{2}}^\pm = \text{constant}$ for still water.

For the well balanced property, we only need to consider the second equation of (1.3). Our well balanced finite volume WENO scheme is given by

$$\Delta x_j \frac{d}{dt} \overline{hu}_j(t) = - \left(\hat{f}_{j+\frac{1}{2}}^l - \hat{f}_{j-\frac{1}{2}}^r \right) + \int_{I_j} g(h, b) dx \tag{4.3}$$

where $\hat{f}_{j+\frac{1}{2}}^l$ and $\hat{f}_{j-\frac{1}{2}}^r$ are the left and right fluxes as defined in Section 3. The residue R is denoted by the right side of the equation (4.3).

Here we also give three conditions which need to be valid for the still water stationary state (1.5):

- We use interpolation to obtain a high order polynomial h_h on the cell I_j , based on the boundary values $h_{j-\frac{1}{2}}^+, h_{j+\frac{1}{2}}^-$ and several other neighboring boundary values. For example, we can use $h_{j+\frac{3}{2}}^-, h_{j+\frac{1}{2}}^-, h_{j-\frac{1}{2}}^+$ and $h_{j-\frac{3}{2}}^+$ to interpolate a third degree polynomial. Similarly, we can use the same interpolation on b to obtain a polynomial b_h , and then use them to compute $\int_{I_j} g(h_h, b_h) dx$ exactly by using a suitable Gauss quadrature. In order to

obtain $(2k)$ -th order accuracy for the approximation of the source term, h_h and b_h need to approximate h and b with $(k + 1)$ -th order accuracy. We observe from the definition of h_h and b_h that the interpolated polynomials satisfy the following properties:

$$h_h(x_{j+\frac{1}{2}}) = h_{j+\frac{1}{2}}^-, \quad h_h(x_{j-\frac{1}{2}}) = h_{j-\frac{1}{2}}^+, \quad b_h(x_{j+\frac{1}{2}}) = b_{j+\frac{1}{2}}^-, \quad b_h(x_{j-\frac{1}{2}}) = b_{j-\frac{1}{2}}^+,$$

$$h_h + b_h = \text{constant} \quad \text{if} \quad h_{j+\frac{1}{2}}^\pm + b_{j+\frac{1}{2}}^\pm = \text{constant}.$$

- We assume that the left and right fluxes $\hat{f}_{j+\frac{1}{2}}^l$ and $\hat{f}_{j-\frac{1}{2}}^r$ satisfy (3.4).
- We assume that interpolated polynomial $U_h(x, t)$ above, is a steady state solution of the equation $(hu)_t + f(U)_x = g(h, b_h)$, where b_h has substituted b . As before, this is true since $h_h + b_h = \text{constant}$ and $(hu)_h = 0$.

Proposition 4.1: Finite volume WENO schemes which satisfy the above three conditions for shallow water equations are well balanced for still water stationary state (1.5).

Proof: If these three conditions are satisfied, the residue R for still water reduces to

$$\begin{aligned} R &= -\hat{f}_{j+\frac{1}{2}}^l + \hat{f}_{j-\frac{1}{2}}^r + \int_{I_j} g(h_h, b_h) dx \\ &= -f(U_h(x_{j+\frac{1}{2}}^-, t)) + f(U_h(x_{j-\frac{1}{2}}^+, t)) + \int_{I_j} g(h_h, b_h) dx \\ &= -\int_{I_j} \partial_x f(U_h) dx + \int_{I_j} g(h_h, b_h) dx \\ &= -\int_{I_j} (\partial_x f(U_h) - g(h_h, b_h)) dx = 0 \end{aligned}$$

where the second equality is due to (3.4), and the last equality follows from (3.5). ■

Note that the first and third conditions are obviously true for the still water of the shallow water equations. As to the second one, we follow Choice B in Section 3, i.e. (3.8), (3.9) and (3.10).

Remark 4.2: During the WENO reconstruction, we reconstruct k polynomials on the cell I_j , based on different stencils, and then define the boundary values $u_{j+\frac{1}{2}}^-$ and $u_{j-\frac{1}{2}}^+$ as convex combinations of those polynomials. We emphasize that such convex combination, when viewed as a function, is *not* a polynomial on I_j , due to the nonlinear nature of the weights. Therefore, the interpolated polynomial u_h is *not* that convex combination and must be recomputed. However, if we use ENO instead of WENO schemes, we can directly take u_h as the ENO reconstructed polynomial on I_j , thereby saving the computational cost to obtain it again by interpolation. ■

Remark 4.3: Audusse et al. [1] introduced a second order well balanced finite volume scheme, and recently, Noelle et al. [21] generalized it to higher order accuracy. The idea proposed here is a generalization of these schemes, by allowing more freedom in defining the polynomials h_h and b_h to save computational cost. If we interpolate h_h and b_h based on the two boundary values plus the center value of the cell I_j (which must be reconstructed), this will give us the fourth order discretization of the source term as introduced in [21]. ■

Now let us consider the 2D shallow water equations (3.13) with the still water stationary solution (3.14) to be balanced. It is straightforward to extend our well balanced WENO schemes to this two-dimensional problem, at least for rectangular meshes. Let us look at the second equation in (3.13) for instance. As we mentioned in Section 2, the numerical scheme is given by:

$$\frac{d}{dt} \bar{u}_{ij}(t) = -\frac{1}{\Delta x_i} \left((\hat{f}_1)_{i+\frac{1}{2},j}^l - (\hat{f}_1)_{i-\frac{1}{2},j}^r \right) - \frac{1}{\Delta y_j} \left((\hat{f}_2)_{i,j+\frac{1}{2}}^l - (\hat{f}_2)_{i,j-\frac{1}{2}}^r \right) + g_{i,j}, \tag{4.4}$$

with

$$(\hat{f}_1)_{i+\frac{1}{2},j}^{l,r} = \sum_{\alpha} w_{\alpha} (\hat{f}_1(\cdot, y_j + \beta_{\alpha} \Delta y_j))_{i+\frac{1}{2}}^{l,r} \tag{4.5}$$

and similarly for $(\hat{f}_2)_{i,j+\frac{1}{2}}^{l,r}$, and

$$\begin{aligned} g_{i,j} &= -\frac{1}{\Delta x_i} \sum_{\alpha} w_{\alpha} \left(\int_{I_i} g(hb_x)(x, y_j + \beta_{\alpha} \Delta y_j) dx \right) \\ &\approx -\frac{1}{\Delta x_i \Delta y_j} \int_{I_i} \int_{I_j} g h b_x dx dy \end{aligned} \tag{4.6}$$

where the first quadrature summation in the y direction must be accurate to the order of the scheme and the integration in the x direction must be computed exactly (by Gauss-quadrature with enough exactness). If the still water stationary solution (3.14) is given, the right side of the numerical scheme (4.4) becomes:

$$\begin{aligned} &-\frac{1}{\Delta x_i} \left((\hat{f}_1)_{i+\frac{1}{2},j}^l - (\hat{f}_1)_{i-\frac{1}{2},j}^r \right) - \frac{1}{\Delta x_i} \sum_{\alpha} w_{\alpha} \left(\int_{I_i} g(hb_x)(x, y_j + \beta_{\alpha} \Delta y_j) dx \right) \\ &= -\frac{1}{\Delta x_i} \sum_{\alpha} w_{\alpha} \left((\hat{f}_1(\cdot, y_j + \beta_{\alpha} \Delta y_j))_{i+\frac{1}{2}}^l - (\hat{f}_1(\cdot, y_j + \beta_{\alpha} \Delta y_j))_{i-\frac{1}{2}}^r \right) \\ &\quad - \frac{1}{\Delta x_i} \sum_{\alpha} w_{\alpha} \left(\int_{I_i} g(hb_x)(x, y_j + \beta_{\alpha} \Delta y_j) dx \right), \end{aligned}$$

We can balance $(\hat{f}_1(\cdot, y_j + \beta_{\alpha} \Delta y_j))_{i+\frac{1}{2}}^l - (\hat{f}_1(\cdot, y_j + \beta_{\alpha} \Delta y_j))_{i-\frac{1}{2}}^r$ with $\int_{I_i} g(hb_x)(x, y_j + \beta_{\alpha} \Delta y_j) dx$ for each fixed α , by the same technique used in the 1D case. This means that at each Gauss point in the y direction, we interpolate polynomials as functions of x , and use them to compute the source term. Well balanced property is thus obtained. Similarly, we can handle the third equation in (3.13) in the same fashion.

Remark 4.4: Both the well-balanced RKDG and finite volume WENO schemes are developed here. The RKDG schemes involve less modification for the well balanced property to hold, and are more flexible for general geometry, adaptivity and parallel implementation. On the other hand, the RKDG schemes rely on limiters to control spurious oscillations for discontinuous solutions, which are less robust than the WENO reconstruction procedure in the capability of maintaining accuracy in smooth regions and controlling oscillations for strong discontinuities simultaneously. We refer to [35] for a comparison of these two types of schemes.

5 Numerical results for the shallow water equations

In this section we provide numerical results to demonstrate the good properties of the well balanced finite volume WENO and finite element RKDG schemes when applied to the shallow water equations. Fifth order finite volume WENO scheme and third order finite element RKDG scheme are implemented as examples. In all numerical tests, time discretization is by the third order TVD Runge-Kutta method in [26]. For finite volume WENO schemes, the CFL number is taken as 0.6, except for the accuracy tests where smaller time steps are taken to ensure that spatial errors dominate. For the third order RKDG scheme, the CFL number is 0.18. For the TVB limiter implemented in the RKDG scheme, the TVB constant M (see [8, 24] for its definition) is taken as 0 in most numerical examples, unless otherwise stated. The gravitation constant g is taken as $9.812m/s^2$ during the computation.

5.1 Test for the exact C-property

The purpose of the first test problem is to verify that the schemes indeed maintain the exact C-property over a non-flat bottom. We choose two different functions for the bottom topography given by ($0 \leq x \leq 10$):

$$b(x) = 5 e^{-\frac{2}{5}(x-5)^2}, \quad (5.1)$$

which is smooth, and

$$b(x) = \begin{cases} 4 & \text{if } 4 \leq x \leq 8 \\ 0 & \text{otherwise,} \end{cases} \quad (5.2)$$

which is discontinuous. The initial data is the stationary solution:

$$h + b = 10, \quad hu = 0.$$

This steady state should be exactly preserved. We compute the solution until $t = 0.5$ using $N = 200$ uniform cells. In order to demonstrate that the exact C-property is indeed maintained up to round-off error, we use single precision, double precision and quadruple precision to perform the computation, and show the L^1 and L^∞ errors for the water height h (note: h in this case is not a constant function!) and the discharge hu in Tables 1 and 2 for the two bottom functions (5.1) and (5.2) and different precisions. For the RKDG method, the errors are computed based on the numerical solutions at cell centers. We can clearly see that the L^1 and L^∞ errors are at the level of round-off errors for different precisions, verifying the exact C-property.

Table 1: L^1 and L^∞ errors for different precisions for the stationary solution with a smooth bottom (5.1).

	precision	L^1 error		L^∞ error	
		h	hu	h	hu
FV	single	3.00E-05	1.10E-04	4.39E-05	5.19E-04
	double	5.04E-14	2.99E-13	1.12E-13	1.26E-12
	quadruple	6.48E-33	3.45E-32	2.17E-32	1.54E-31
RKDG	single	8.41E-06	3.15E-05	3.72E-05	2.06E-04
	double	3.02E-15	3.59E-15	1.60E-14	7.22E-14
	quadruple	8.06E-31	2.92E-33	8.05E-29	1.07E-31

Table 2: L^1 and L^∞ errors for different precisions for the stationary solution with a nonsmooth bottom (5.2).

	precision	L^1 error		L^∞ error	
		h	hu	h	hu
FV	single	1.80E-05	1.40E-04	3.24E-05	2.41E-04
	double	4.41E-14	2.57E-13	1.05E-13	1.30E-12
	quadruple	4.27E-32	3.71E-31	1.07E-31	1.46E-30
RKDG	single	5.72E-07	1.22E-07	9.54E-07	3.41E-07
	double	1.40E-15	3.16E-16	3.55E-15	7.77E-15
	quadruple	8.06E-31	1.65E-34	8.06E-29	4.12E-33

We have also computed stationary solutions using initial conditions which are not the still water stationary solutions and letting time evolve into a still water stationary solution, obtaining similar results with the exact C-property, i.e. the errors are at the level of round-off errors for different precisions.

5.2 Testing the orders of accuracy

In this example we will test the high order accuracy of our schemes for a smooth solution. We have the following bottom function and initial conditions

$$b(x) = \sin^2(\pi x), \quad h(x, 0) = 5 + e^{\cos(2\pi x)}, \quad (hu)(x, 0) = \sin(\cos(2\pi x)), \quad x \in [0, 1]$$

with periodic boundary conditions, see [31]. Since the exact solution is not known explicitly for this case, we use the fifth order finite volume WENO scheme with $N = 12, 800$ cells to compute a reference solution, and treat this reference solution as the exact solution in computing the numerical errors. We compute up to $t = 0.1$ when the solution is still smooth (shocks develop later in time for this problem). Table 3 contains the L^1 errors for the cell averages and numerical orders of accuracy for the finite volume and RKDG schemes, respectively. We can clearly see

Table 3: L^1 errors and numerical orders of accuracy for the example in Section 5.2.

No. of cells	FV schemes					RKDG schemes			
	CFL	h		hu		h		hu	
		L^1 error	order	L^1 error	order	L^1 error	order	L^1 error	order
25	0.6	1.28E-02		1.16E-01		2.35E-03		2.12E-02	
50	0.6	2.25E-03	2.50	2.25E-02	2.37	1.14E-04	4.36	1.01E-03	4.39
100	0.4	3.26E-04	2.79	2.75E-03	3.03	1.24E-05	3.20	1.09E-04	3.21
200	0.3	2.33E-05	3.80	2.00E-04	3.79	1.02E-06	3.59	8.97E-06	3.60
400	0.2	9.54E-07	4.61	8.20E-06	4.60	1.12E-07	3.19	9.79E-07	3.19
800	0.1	2.99E-08	4.99	2.58E-07	4.99	1.30E-08	3.09	1.14E-07	3.08

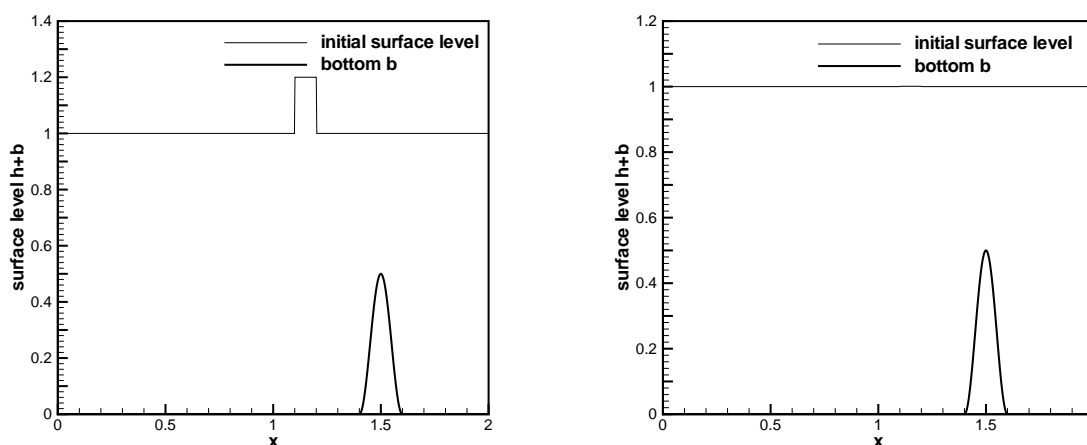


Figure 1: The initial surface level $h + b$ and the bottom b for a small perturbation of a steady-state water. Left: a big pulse $\epsilon=0.2$; right: a small pulse $\epsilon=0.001$.

that fifth order accuracy is achieved for the WENO scheme, and third order accuracy is achieved for the RKDG scheme. For the RKDG scheme, the TVB constant M is taken as 32. Notice that the CFL number we have used for the finite volume scheme decreases with the mesh size and is recorded in Table 3. For the RKDG method, the CFL number is fixed at 0.18.

5.3 A small perturbation of a steady-state water

The following quasi-stationary test case was proposed by LeVeque [19]. It was chosen to demonstrate the capability of the proposed scheme for computations on a rapidly varying flow over a smooth bed, and the perturbation of a stationary state.

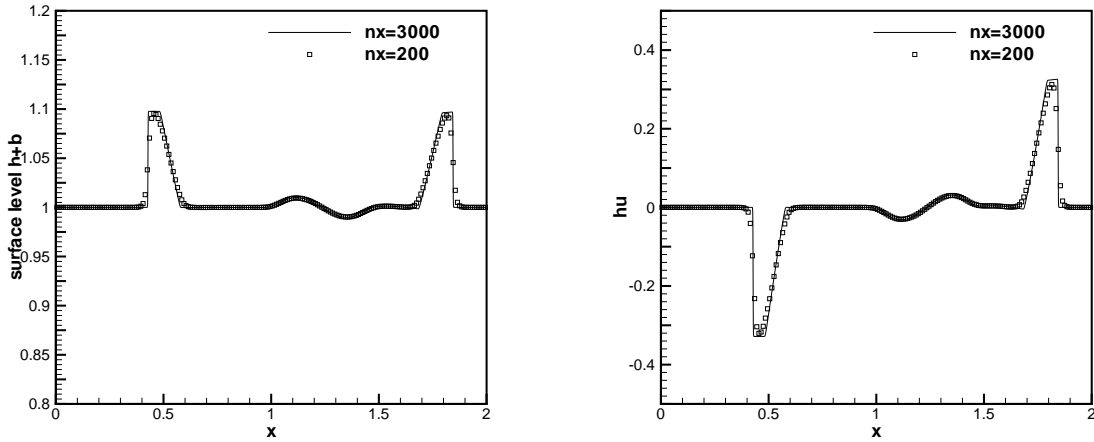


Figure 2: FV scheme: Small perturbation of a steady-state water with a big pulse. $t=0.2s$. Left: surface level $h + b$; right: the discharge hu .

The bottom topography consists of one hump:

$$b(x) = \begin{cases} 0.25(\cos(10\pi(x - 1.5)) + 1) & \text{if } 1.4 \leq x \leq 1.6 \\ 0 & \text{otherwise} \end{cases} \quad (5.3)$$

The initial conditions are given with

$$(hu)(x, 0) = 0 \quad \text{and} \quad h(x, 0) = \begin{cases} 1 - b(x) + \epsilon & \text{if } 1.1 \leq x \leq 1.2 \\ 1 - b(x) & \text{otherwise} \end{cases} \quad (5.4)$$

where ϵ is a non-zero perturbation constant. Two cases have been run: $\epsilon = 0.2$ (big pulse) and $\epsilon = 0.001$ (small pulse). Theoretically, for small ϵ , this disturbance should split into two waves, propagating left and right at the characteristic speeds $\pm\sqrt{gh}$. Many numerical methods have difficulty with the calculations involving such small perturbations of the water surface [19]. Both sets of initial conditions are shown in Figure 1. The solution at time $t=0.2s$ for the big pulse $\epsilon = 0.2$, obtained on a 200 cell uniform grid with simple transmissive boundary conditions, and compared with a 3000 cell solution, is shown in Figure 2 for the FV scheme and in Figure 4 for the RKDG scheme. The results for the small pulse $\epsilon = 0.001$ are shown in Figures 3 and 5. At this time, the downstream-traveling water pulse has already passed the bump. We can clearly see that there are no spurious numerical oscillations.

5.4 The dam breaking problem over a rectangular bump

In this example we simulate the dam breaking problem over a rectangular bump, which involves a rapidly varying flow over a discontinuous bottom topography. This example was used in [29].

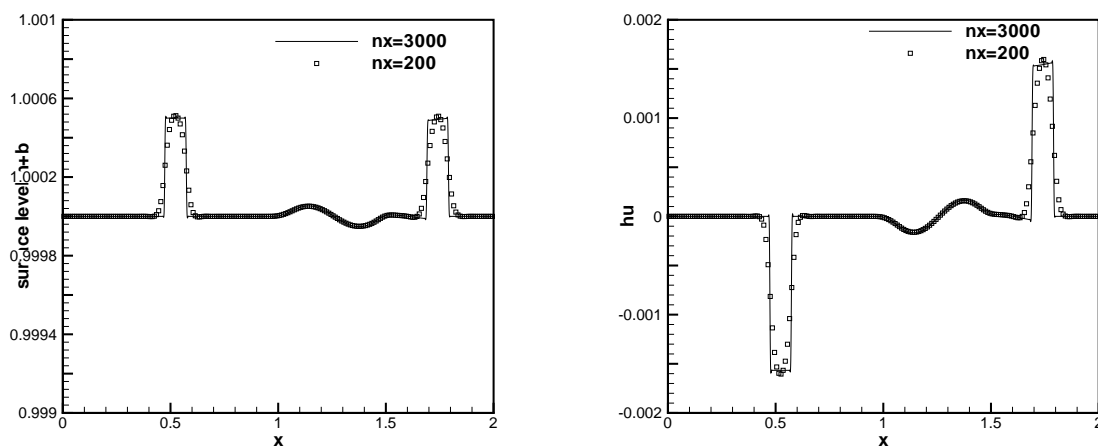


Figure 3: FV scheme: Small perturbation of a steady-state water with a small pulse. $t=0.2s$. Left: surface level $h + b$; right: the discharge hu .

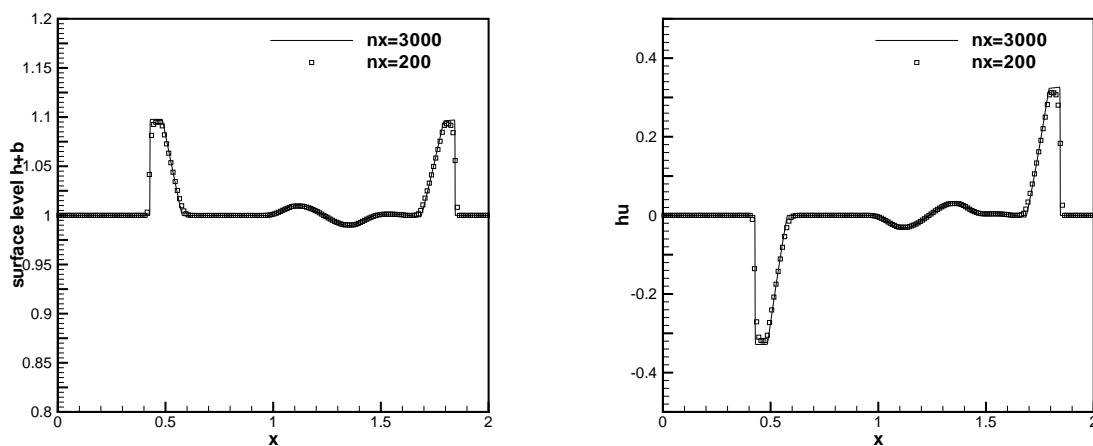


Figure 4: RKDG scheme: Small perturbation of a steady-state water with a big pulse. $t=0.2s$. Left: surface level $h + b$; right: the discharge hu .

The bottom topography takes the form:

$$b(x) = \begin{cases} 8 & \text{if } |x - 750| \leq 1500/8 \\ 0 & \text{otherwise} \end{cases} \tag{5.5}$$

for $x \in [0, 1500]$. The initial conditions are

$$(hu)(x, 0) = 0 \quad \text{and} \quad h(x, 0) = \begin{cases} 20 - b(x) & \text{if } x \leq 750 \\ 15 - b(x) & \text{otherwise} \end{cases} \tag{5.6}$$

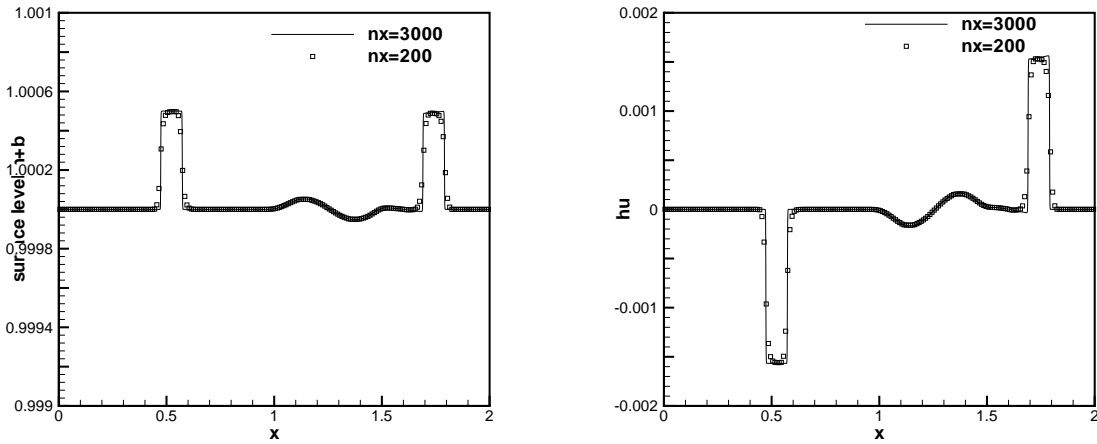


Figure 5: RKDG scheme: Small perturbation of a steady-state water with a small pulse. $t=0.2s$. Left: surface level $h + b$; right: the discharge hu .

The numerical results obtained by the FV scheme with 400 uniform cells (and a comparison with the results using 4000 uniform cells) are shown in Figures 6 and 7, with two different ending time $t=15s$ and $t=60s$. Figures 8 and 9 demonstrate the numerical results by the RKDG scheme, with the same number of uniform cells. In this example, the water height $h(x)$ is discontinuous at the points $x = 562.5$ and $x = 937.5$, while the surface level $h(x) + b(x)$ is smooth there. Both schemes work well for this example, giving well resolved, non-oscillatory solutions using 400 cells which agree with the converged results using 4000 cells.

5.5 Steady flow over a hump

The purpose of this test case is to study the convergence in time towards steady flow over a bump. These are classical test problems for transcritical and subcritical flows, and they are widely used to test numerical schemes for shallow water equations. For example, they have been considered by the *working group on dam break modelling* [12], and have been used as a test case in, e.g. [28].

The bottom function is given by:

$$b(x) = \begin{cases} 0.2 - 0.05(x - 10)^2 & \text{if } 8 \leq x \leq 12 \\ 0 & \text{otherwise} \end{cases} \quad (5.7)$$

for a channel of length $25m$. The initial conditions are taken as

$$h(x, 0) = 0.5 - b(x) \quad \text{and} \quad u(x, 0) = 0.$$

Depending on different boundary conditions, the flow can be subcritical or transcritical with or without a steady shock. The computational parameters common for all three cases are: uniform

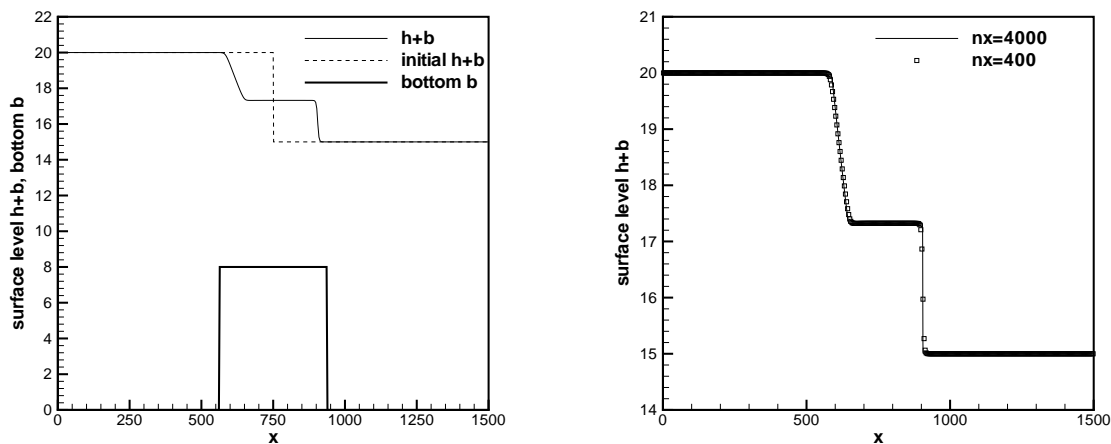


Figure 6: FV scheme: The surface level $h + b$ for the dam breaking problem at time $t=15s$. Left: the numerical solution using 400 grid cells, plotted with the initial condition and the bottom topography; Right: the numerical solution using 400 and 4000 grid cells.

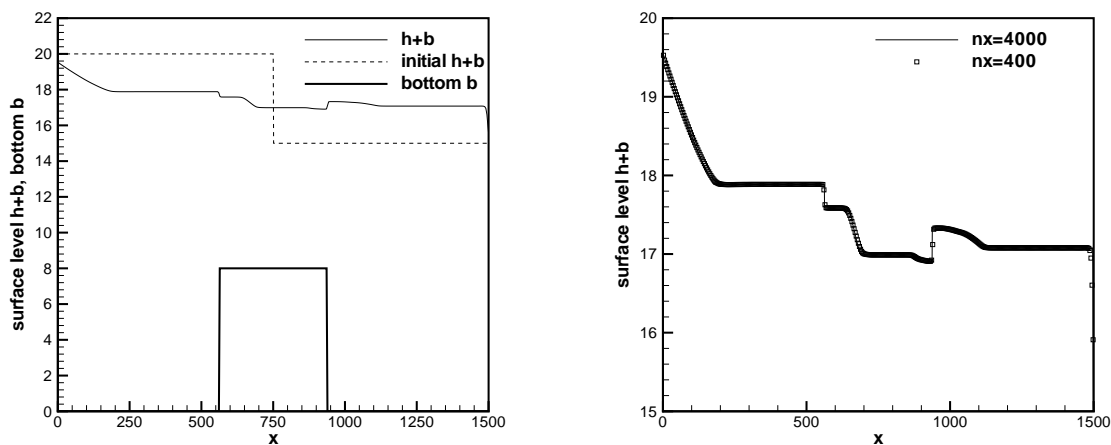


Figure 7: FV scheme: The surface level $h + b$ for the dam breaking problem at time $t=60s$. Left: the numerical solution using 400 grid cells, plotted with the initial condition and the bottom topography; Right: the numerical solution using 400 and 4000 grid cells.

mesh size $\Delta x = 0.125 \text{ m}$ (200 cells), ending time $t = 200 \text{ s}$. Analytical solutions for the various cases are given in Goutal and Maurel [12].

a): Transcritical flow without a shock.

- upstream: The discharge $hu=1.53 \text{ m}^2/s$ is imposed.

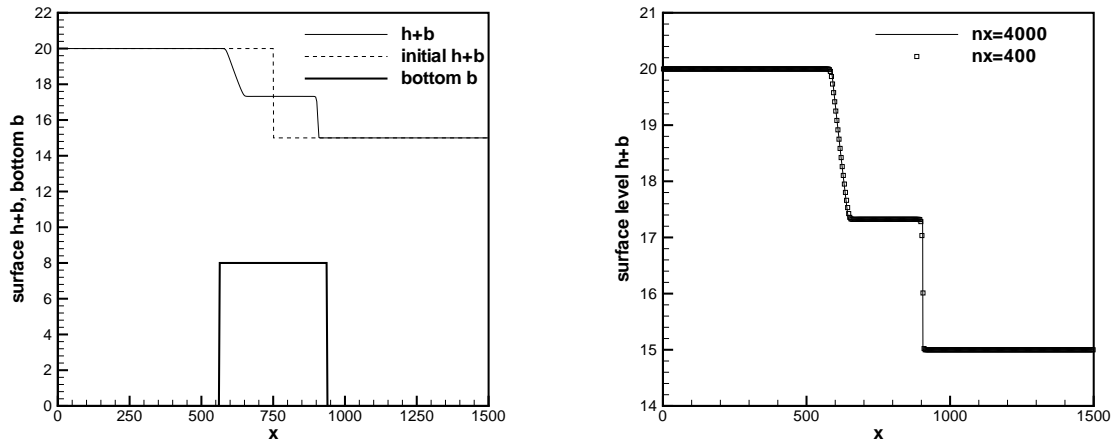


Figure 8: RKDG scheme: The surface level $h + b$ for the dam breaking problem at time $t=15s$. Left: the numerical solution using 400 grid cells, plotted with the initial condition and the bottom topography; Right: the numerical solution using 400 and 4000 grid cells.

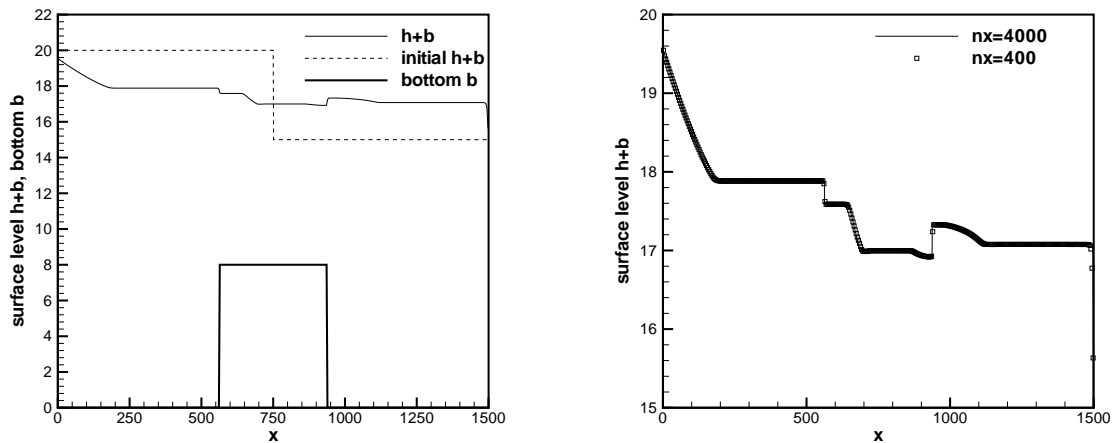


Figure 9: RKDG scheme: The surface level $h + b$ for the dam breaking problem at time $t=60s$. Left: the numerical solution using 400 grid cells, plotted with the initial condition and the bottom topography; Right: the numerical solution using 400 and 4000 grid cells.

- downstream: The water height $h=0.66 m$ is imposed when the flow is subcritical.

The surface level $h + b$ and the discharge hu , as the numerical flux for the water height h in equation (1.3), are plotted in Figures 10 and 11, which show very good agreement with the analytical solution. The correct capturing of the discharge hu is usually more difficult than the surface level $h + b$, as noticed by many authors.

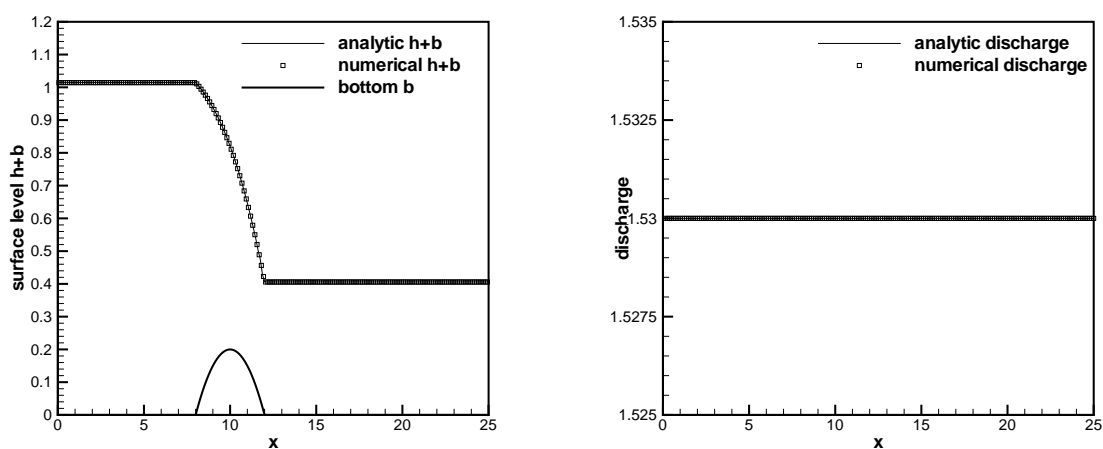


Figure 10: FV scheme: Steady transcritical flow over a bump without a shock. Left: the surface level $h + b$; right: the discharge hu as the numerical flux for the water height h .

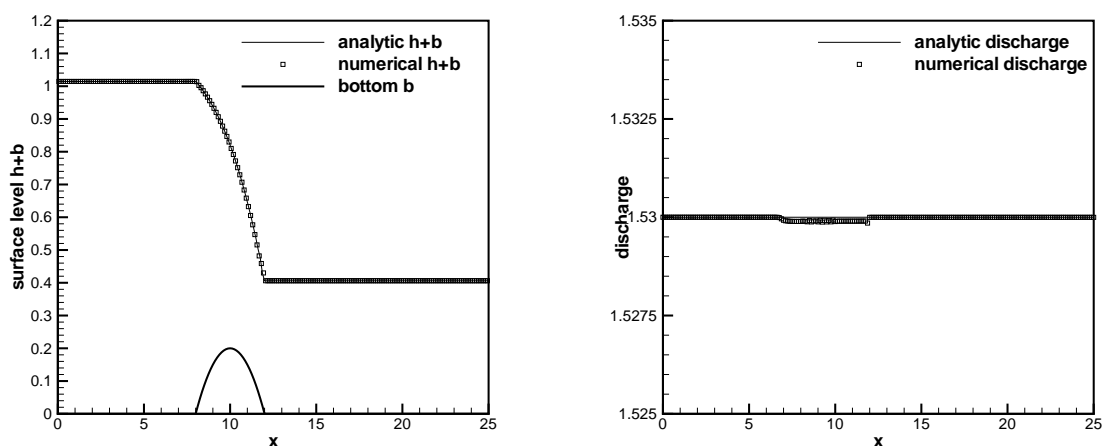


Figure 11: RKDG scheme: Steady transcritical flow over a bump without a shock. Left: the surface level $h + b$; right: the discharge hu as the numerical flux for the water height h .

b): Transcritical flow with a shock.

- upstream: The discharge $hu=0.18 \text{ m}^2/\text{s}$ is imposed.
- downstream: The water height $h=0.33 \text{ m}$ is imposed.

In this case, the Froude number $Fr = u/\sqrt{gh}$ increases to a value larger than one above the bump, and then decreases to less than one. A stationary shock can appear on the surface. The surface level $h + b$ and the discharge hu , as the numerical flux for the water height h in equation

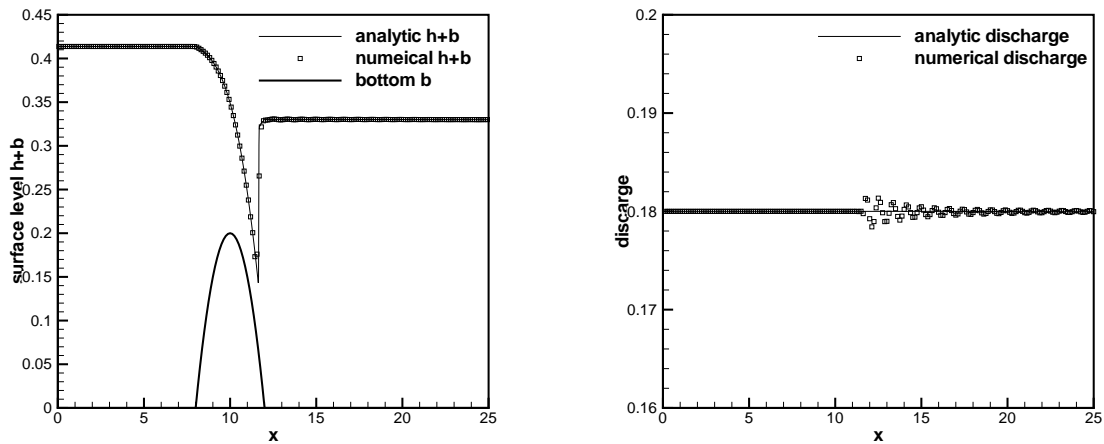


Figure 12: FV scheme: Steady transcritical flow over a bump with a shock. Left: the surface level $h + b$; right: the discharge hu as the numerical flux for the water height h .

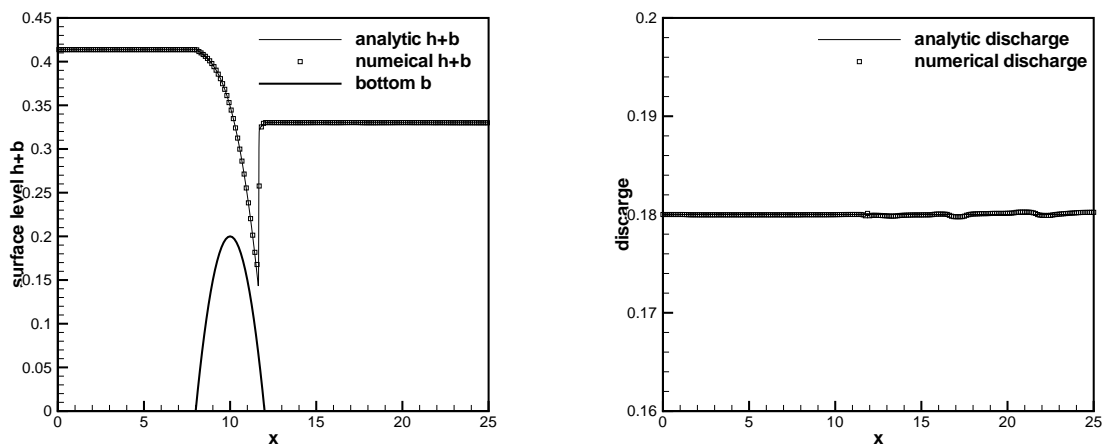


Figure 13: RKDG scheme: Steady transcritical flow over a bump with a shock. Left: the surface level $h + b$; right: the discharge hu as the numerical flux for the water height h .

(1.3), are plotted in Figure 12 and 13. In Figure 12 for the FV scheme, some minor oscillations can be observed near the jump. Here we also plot the numerical result with 400 uniform cells in Figure 14, where we can observe that the oscillation is completely removed. The reason for this phenomenon is still not known.

c): Subcritical flow.

- upstream: The discharge $hu=4.42 \text{ m}^2/\text{s}$ is imposed.

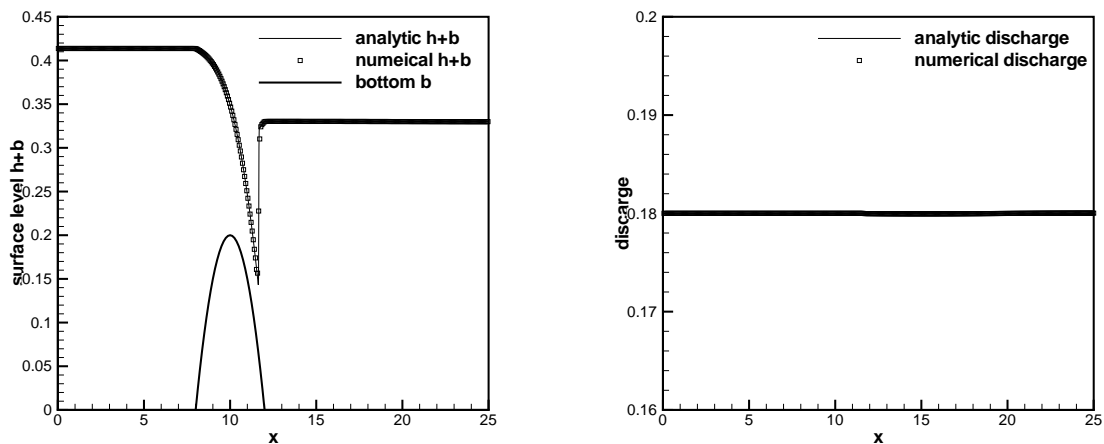


Figure 14: FV scheme with 400 uniform cells: Steady transcritical flow over a bump with a shock. Left: the surface level $h + b$; right: the discharge hu as the numerical flux for the water height h .

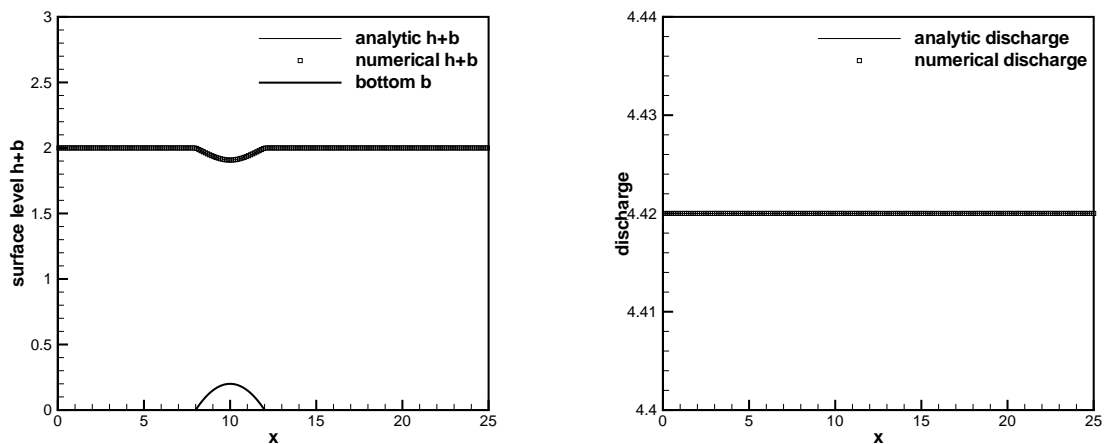


Figure 15: FV scheme: Steady subcritical flow over a bump. Left: the surface level $h + b$; right: the discharge hu as the numerical flux for the water height h .

- downstream: The water height $h=2\text{ m}$ is imposed.

This is a subcritical flow. The surface level $h + b$ and the discharge hu , as the numerical flux for the water height h in equation (1.3), are plotted in Figure 15 and 16, which are in good agreement with the analytical solution.

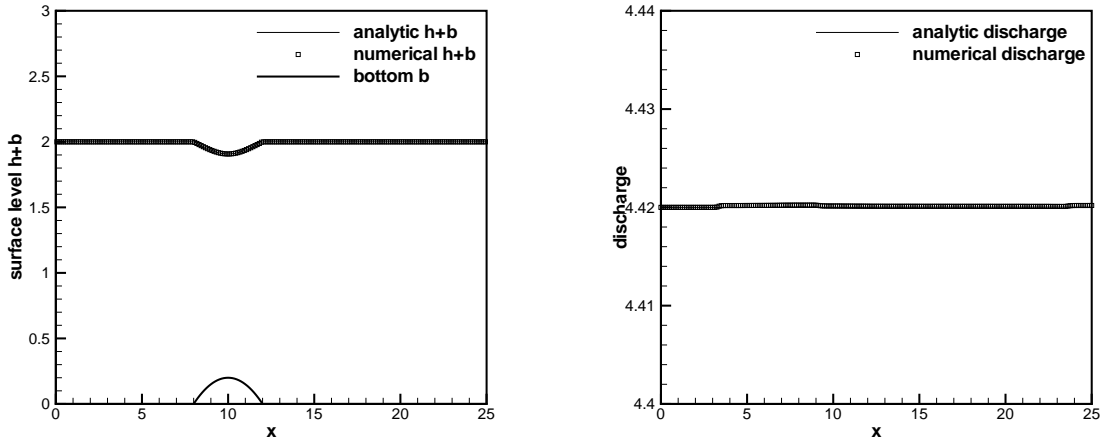


Figure 16: RKDG scheme: Steady subcritical flow over a bump. Left: the surface level $h + b$; right: the discharge hu as the numerical flux for the water height h .

5.6 Test for the exact C-property in two dimensions

This example is used to check that our schemes indeed maintain the exact C-property over a non-flat bottom for 2D shallow water equations. The two-dimensional hump

$$b(x, y) = 0.8e^{-50((x-0.5)^2+(y-0.5)^2)}, \quad x, y \in [0, 1] \quad (5.8)$$

is chosen to be the bottom. $h(x, y, 0) = 1 - b(x, y)$ is the initial depth of the water. Initial velocity is set to be zero. This surface should remain flat. The computation is performed to $t = 0.1$ using single, double and quadruple precisions with a 100×100 uniform mesh. Table 4 contains the L^1 errors for the water height h (which is not a constant function) and the discharges hu and hv for both schemes. We can clearly see that the L^1 errors are at the level of round-off errors for different precisions, verifying the exact C-property.

5.7 Testing the orders of accuracy

In this example we check the numerical orders of accuracy when the schemes are applied to the following two dimensional problem. The bottom topography and the initial data are given by:

$$\begin{aligned} b(x, y) &= \sin(2\pi x) + \cos(2\pi y), & h(x, y, 0) &= 10 + e^{\sin(2\pi x)} \cos(2\pi y), \\ (hu)(x, y, 0) &= \sin(\cos(2\pi x)) \sin(2\pi y), & (hv)(x, y, 0) &= \cos(2\pi x) \cos(\sin(2\pi y)) \end{aligned}$$

defined over a unit square, with periodic boundary conditions. The terminal time is taken as $t=0.05$ to avoid the appearance of shocks in the solution. Since the exact solution is also not known explicitly for this case, we use the same fifth order WENO scheme with an extremely refined mesh consisting of 1600×1600 cells to compute a reference solution, and treat this

Table 4: L^1 errors for different precisions for the stationary solution in Section 5.6.

	precision	L^1 error		
		h	hu	hv
FV	single	8.77E-07	7.49E-07	6.93E-07
	double	1.49E-15	2.31E-15	2.30E-15
	quadruple	1.04E-33	9.87E-34	1.01E-33
RKDG	single	9.43E-08	4.84E-07	4.94E-07
	double	6.98E-17	2.31E-15	2.31E-15
	quadruple	6.14E-34	1.52E-33	1.53E-33

Table 5: FV scheme: L^1 errors and numerical orders of accuracy for the example in Section 5.7.

Number of cells	CFL	h		hu		hv	
		L^1 error	order	L^1 error	order	L^1 error	order
25×25	0.6	7.91E-03		2.12E-02		6.52E-02	
50×50	0.6	1.13E-03	2.81	2.01E-03	3.40	9.22E-03	2.82
100×100	0.6	8.89E-05	3.66	1.25E-04	4.00	7.19E-04	3.68
200×200	0.4	4.07E-06	4.45	5.19E-06	4.59	3.30E-05	4.45
400×400	0.3	1.42E-07	4.84	1.84E-07	4.82	1.15E-06	4.84
800×800	0.2	4.38E-09	5.02	5.99E-09	4.94	3.63E-08	4.99

reference solution as the exact solution in computing the numerical errors. The TVB constant M in the limiter for the RKDG scheme is taken as 40 here. Tables 5 and 6 contain the L^1 errors and orders of accuracy for the cell averages. We can clearly see that, in this two dimensional test case, fifth order accuracy is achieved for the finite volume WENO scheme and close to third order accuracy is achieved for the RKDG scheme.

5.8 A small perturbation of a two dimensional steady-state water

This is a classical example to show the capability of the proposed scheme for the perturbation of the stationary state, given by LeVeque [19]. It is analogous to the test done previously in Section 5.3 in one dimension.

We solve the system in the rectangular domain $[0, 2] \times [0, 1]$. The bottom topography is an isolated elliptical shaped hump:

$$b(x, y) = 0.8 e^{-5(x-0.9)^2 - 50(y-0.5)^2}. \quad (5.9)$$

Table 6: RKDG scheme: L^1 errors and numerical orders of accuracy for the example in Section 5.7.

Number of cells	h		hu		hv	
	L^1 error	order	L^1 error	order	L^1 error	order
25×25	2.45E-03		1.36E-02		2.05E-02	
50×50	5.73E-04	2.10	2.92E-03	2.22	4.75E-03	2.11
100×100	1.06E-04	2.43	5.31E-04	2.46	8.51E-04	2.48
200×200	1.71E-05	2.63	8.81E-05	2.60	1.39E-04	2.61
400×400	2.53E-06	2.75	1.32E-05	2.74	2.11E-05	2.72
800×800	3.52E-07	2.84	1.88E-06	2.81	3.01E-06	2.81

The surface is initially given by:

$$\begin{aligned}
 h(x, y, 0) &= \begin{cases} 1 - b(x, y) + 0.01 & \text{if } 0.05 \leq x \leq 0.15 \\ 1 - b(x, y) & \text{otherwise} \end{cases} \\
 hu(x, y, 0) &= hv(x, y, 0) = 0
 \end{aligned} \tag{5.10}$$

So the surface is almost flat except for $0.05 \leq x \leq 0.15$, where h is perturbed upward by 0.01. Figures 17 and 18 display the right-going disturbance as it propagates past the hump, on two different uniform meshes with 200×100 cells and 600×300 cells for comparison. The surface level $h + b$ is presented at different times. The results indicate that both schemes can resolve the complex small features of the flow very well.

6 Other applications

In this section, we generalize high order well balanced schemes, designed in Sections 3 and 4, to other balance laws introduced in [32], including the elastic wave equation, the hyperbolic model for a chemosensitive movement, the nozzle flow, a model of fluid mechanics and a two phase flow model. Due to page limitation, only the elastic wave equation and chemosensitive movement model are investigated here, however our technique can also be applied to the other three cases. Some selective numerical tests are presented to show the good properties of our well balance schemes.

6.1 Elastic wave equation

We consider the propagation of compressional waves [2, 30] in an one-dimensional elastic rod with a given media density $\rho(x)$. The equations of motion in a Lagrangian frame are given by the balance laws:

$$\begin{cases} (\rho\varepsilon)_t + (-\rho u)_x = -u \frac{d\rho}{dx} \\ (\rho u)_t + (-\sigma)_x = 0, \end{cases} \tag{6.1}$$

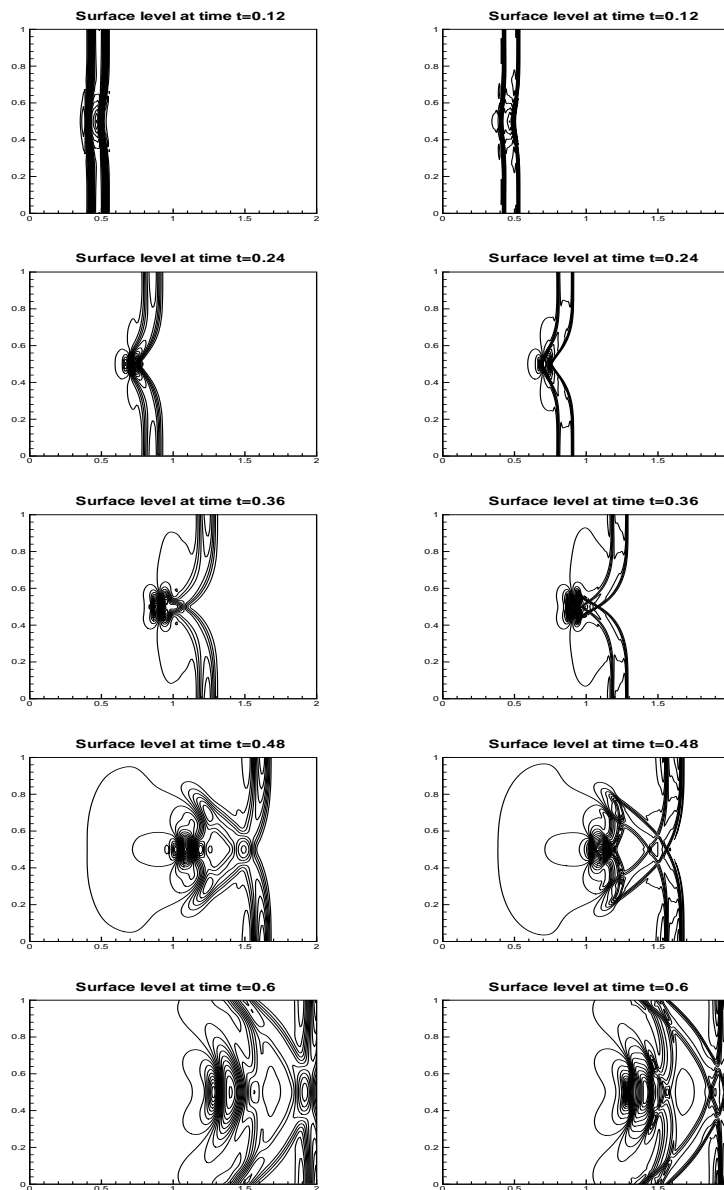


Figure 17: FV scheme: The contours of the surface level $h+b$ for the problem in Section 5.8. 30 uniformly spaced contour lines. From top to bottom: at time $t = 0.12$ from 0.99942 to 1.00656; at time $t = 0.24$ from 0.99318 to 1.01659; at time $t = 0.36$ from 0.98814 to 1.01161; at time $t = 0.48$ from 0.99023 to 1.00508; and at time $t = 0.6$ from 0.99514 to 1.00629. Left: results with a 200×100 uniform mesh. Right: results with a 600×300 uniform mesh.

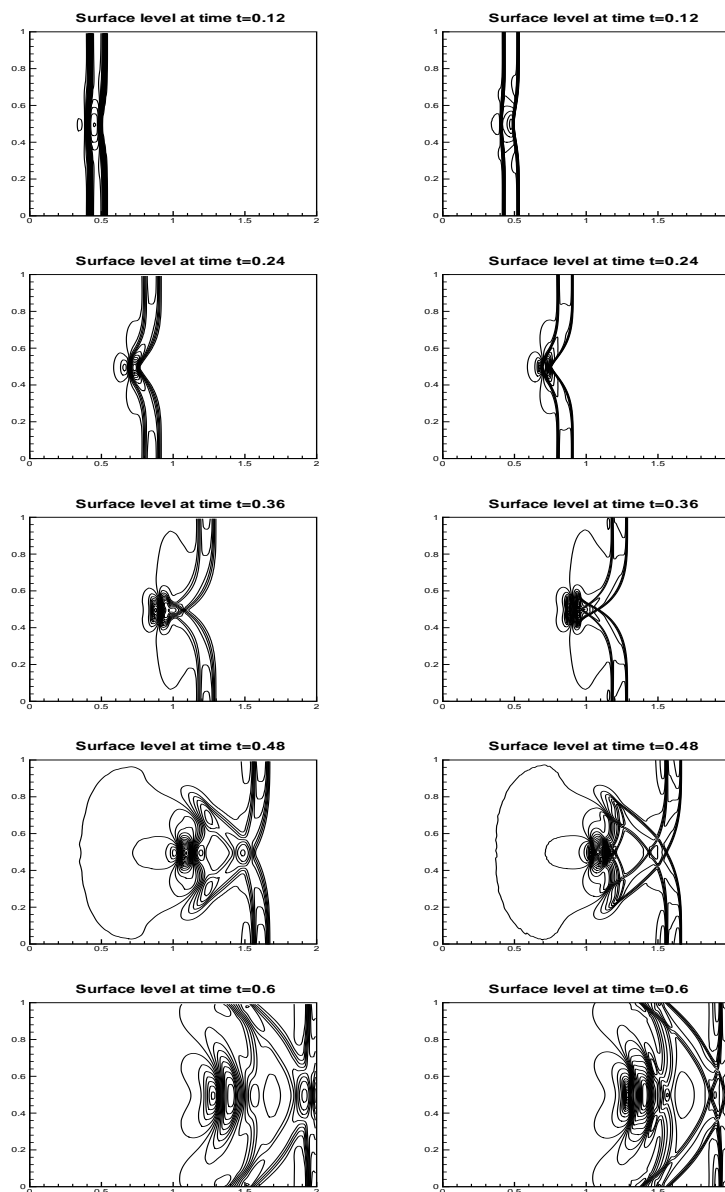


Figure 18: RKDG scheme: The contours of the surface level $h + b$ for the problem in Section 5.8. 30 uniformly spaced contour lines. From top to bottom: at time $t = 0.12$ from 0.99942 to 1.00656; at time $t = 0.24$ from 0.99318 to 1.01659; at time $t = 0.36$ from 0.98814 to 1.01161; at time $t = 0.48$ from 0.99023 to 1.00508; and at time $t = 0.6$ from 0.99514 to 1.00629. Left: results with a 200×100 uniform mesh. Right: results with a 600×300 uniform mesh.

where ε is the strain, u is the velocity and σ is a given stress-strain relationship $\sigma(\varepsilon, x)$. The equation of linear acoustics can be obtained from above if the stress-strain relationship is linear,

$$\sigma(\varepsilon, x) = K(x) \varepsilon$$

where $K(x)$ is the given bulk modulus of compressibility. The steady state we are interested to preserve for this problem is characterized by

$$a_1 \equiv \sigma(\varepsilon, x) = \text{constant}, \quad a_2 \equiv u = \text{constant}.$$

Here we only show the well balanced property for the RKDG schemes. Similar idea can be used for the finite volume WENO schemes.

First, we project the initial value to obtain $U_h = ((\rho\varepsilon)_h, (\rho u)_h)^T$, and also apply the same procedure for ρ to obtain ρ_h . Then, we check the three conditions in Section 3 one by one. Only the first equation in (6.1) must be considered for the well balanced property.

1: If the steady state is reached, $u_h \equiv \frac{(\rho u)_h}{\rho_h}$ is constant and ρ_h is a polynomial, hence the integral of the source term can be calculated exactly.

2: We set

$$(\rho u)_{h,j+\frac{1}{2}}^{*,+} = \frac{(\rho u)_{h,j+\frac{1}{2}}^+}{\rho_{h,j+\frac{1}{2}}^+} \max(\rho_{h,j+\frac{1}{2}}^+, \rho_{h,j+\frac{1}{2}}^-) \tag{6.2}$$

$$(\rho u)_{h,j+\frac{1}{2}}^{*,-} = \frac{(\rho u)_{h,j+\frac{1}{2}}^-}{\rho_{h,j+\frac{1}{2}}^-} \max(\rho_{h,j+\frac{1}{2}}^+, \rho_{h,j+\frac{1}{2}}^-) \tag{6.3}$$

and redefine the left and right values of U as:

$$U_{h,j+\frac{1}{2}}^{*,\pm} = \begin{pmatrix} (\rho\varepsilon)_{h,j+\frac{1}{2}}^\pm \\ (\rho u)_{h,j+\frac{1}{2}}^{*,\pm} \end{pmatrix} \tag{6.4}$$

Then we define the left and right fluxes as:

$$\hat{f}_{j+\frac{1}{2}}^l = F(U_{h,j+\frac{1}{2}}^{*,-}, U_{h,j+\frac{1}{2}}^{*,+}) + \begin{pmatrix} -(\rho u)_{h,j+\frac{1}{2}}^- + (\rho u)_{h,j+\frac{1}{2}}^{*,-} \\ 0 \end{pmatrix} \tag{6.5}$$

$$\hat{f}_{j-\frac{1}{2}}^r = F(U_{h,j-\frac{1}{2}}^{*,-}, U_{h,j-\frac{1}{2}}^{*,+}) + \begin{pmatrix} -(\rho u)_{h,j-\frac{1}{2}}^+ + (\rho u)_{h,j-\frac{1}{2}}^{*,+} \\ 0 \end{pmatrix}. \tag{6.6}$$

The max in (6.2)-(6.3) was chosen in [1] to guarantee positive water height and was referred to as ‘‘hydrostatic reconstruction’’ there. Here it does not have a clear physical meaning and could be replaced by minimum or average as well.

3: $(\rho u)_h$, satisfying $u_h = \text{constant}$, is also a steady state solution of :

$$(-\rho u)_x = -u \frac{d\rho_h}{dx}.$$

With these three conditions, we can repeat the proof of Proposition 3.1 to show that our schemes are indeed well balanced and high order accurate.

Remark 6.1: When performing the limiting on the function $(\rho u)_h$ after each Runge-Kutta stage to control spurious oscillations, we keep in mind that our purpose is to maintain the steady state solution $(\rho u)_h$ which satisfies $u_h = \text{constant}$. Here we follow the idea used in [33], and first check whether any limiting is needed based on the function u_h in each Runge-Kutta stage. If the answer is yes, then the actual limiter is implemented on $(\rho u)_h$. ■

Next, we present the numerical result for a linear acoustic test [2]. The properties of the media are given by

$$c(x) = \sqrt{\frac{K(x)}{\rho(x)}} = 1 + 0.5 \sin(10\pi x), \quad Z(x) = \rho(x)c(x) = 1 + 0.25 \cos(10\pi x).$$

The initial conditions are given by

$$\rho \varepsilon(x, 0) = \begin{cases} \frac{-1.75 + 0.75 \cos(10\pi x)}{c^2(x)}, & \text{if } 0.4 < x < 0.6 \\ \frac{-1}{c^2(x)}, & \text{otherwise} \end{cases}, \quad u(x, 0) = 0.$$

It is test cases where the impedance $Z(x)$ and hence the eigenvectors are both spatially varying. We perform the computation with 200 uniform cells, with the ending time $t = 0.4s$. An “exact” reference solution is computed with the same scheme over a 2000 grid point uniform cells. The simulation results are shown in Figure 19. The numerical resolution shows very good agreement with the “exact” reference solution.

6.2 Chemosensitive movement

Originated from biology, chemosensitive movement [11, 14] is a process by which cells change their direction reacting to the presence of a chemical substance, approaching chemically favorable environments and avoiding unfavorable ones. Hyperbolic models for chemotaxis are recently introduced [14] and take the form

$$\begin{cases} n_t + (nu)_x = 0 \\ (nu)_t + (nu^2 + n)_x = n\chi'(c)\frac{\partial c}{\partial x} - \sigma nu \end{cases} \quad (6.7)$$

where the chemical concentration $c = c(x, t)$ is given by the parabolic equation

$$\frac{\partial c}{\partial t} - D_c \Delta c = n - c.$$

Here, $n(x, t)$ is the cell density, $nu(x, t)$ is the population flux and σ is the friction coefficient.

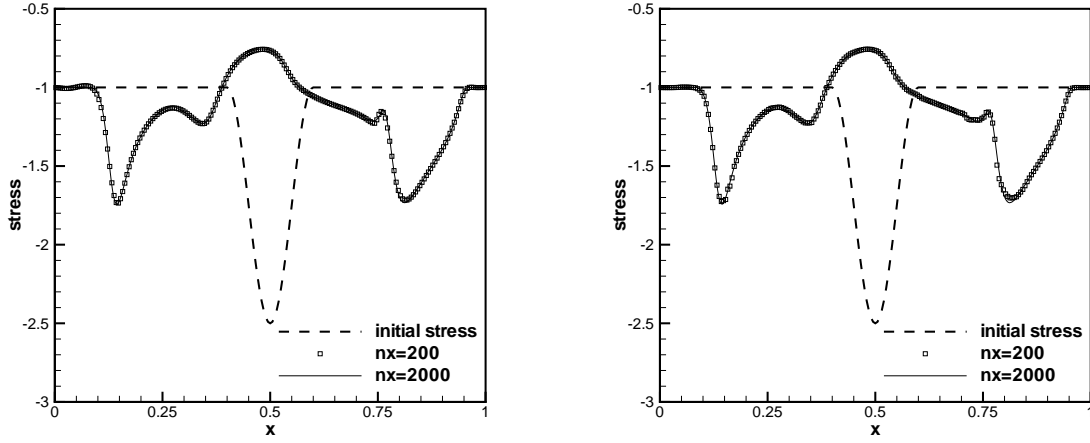


Figure 19: The numerical (symbols) and the “exact” reference (solid line) stress $\sigma(x)$ at time $t = 0.4s$. Left: FV schemes; right: DG schemes.

We would like to preserve the steady state solution to (6.7) with a zero population flux, which satisfies

$$\frac{n}{e^{\chi(c)}} = constant, \quad nu = 0. \tag{6.8}$$

where $c = c(x)$ does not depend on t in steady state.

Here we only show the well balanced property for the RKDG schemes. Similar idea can be used for the finite volume WENO schemes.

First, we project the initial value to obtain $U_h = (n_h, (nu)_h)^T$, and also project $e^{\chi(c)}$ to obtain $(e^{\chi(c)})_h$. Then, we check the three conditions in Section 3 one by one. Only the second equation in (6.7) is relevant for the well balanced property.

1: The source term can be written as: $\frac{n}{e^{\chi(c)}} \frac{d}{dx} e^{\chi(c)} - \sigma nu$. If the steady state is reached, $\frac{n}{e^{\chi(c)}}$ is constant and $(e^{\chi(c)})_h$ is a polynomial, hence the integral of the source term can be calculated exactly.

2: We set

$$n_{h,j+\frac{1}{2}}^{*,+} = \frac{n_{h,j+\frac{1}{2}}^+}{(e^{\chi(c)})_{h,j+\frac{1}{2}}^+} \max((e^{\chi(c)})_{h,j+\frac{1}{2}}^+, (e^{\chi(c)})_{h,j+\frac{1}{2}}^-) \tag{6.9}$$

$$n_{h,j+\frac{1}{2}}^{*,-} = \frac{n_{h,j+\frac{1}{2}}^-}{(e^{\chi(c)})_{h,j+\frac{1}{2}}^-} \max((e^{\chi(c)})_{h,j+\frac{1}{2}}^+, (e^{\chi(c)})_{h,j+\frac{1}{2}}^-) \tag{6.10}$$

and redefine the left and right values of U as:

$$U_{h,j+\frac{1}{2}}^{*,\pm} = \begin{pmatrix} n_{h,j+\frac{1}{2}}^{*,\pm} \\ (nu)_{h,j+\frac{1}{2}}^{\pm} \end{pmatrix} \tag{6.11}$$

Table 7: L^1 errors and numerical orders of accuracy for the example in Section 6.2.

No. of points	FV schemes						DG schemes			
	CFL	$\rho\epsilon$		ρu		$\rho\epsilon$		ρu		
		L^1 error	order	L^1 error	order	L^1 error	order	L^1 error	order	
20	0.6	1.10E-002		8.76E-003		1.13E-004		1.13E-004		
40	0.6	1.20E-003	3.20	1.02E-003	3.10	1.56E-005	2.86	1.42E-005	2.99	
80	0.5	1.19E-004	3.34	9.81E-005	3.38	1.06E-006	3.88	9.58E-007	3.89	
160	0.4	6.27E-006	4.25	5.32E-006	4.20	8.91E-008	3.57	8.09E-008	3.56	
320	0.3	2.48E-007	4.66	2.12E-007	4.65	8.93E-009	3.32	8.10E-009	3.32	
640	0.1	8.09E-009	4.95	6.85E-008	4.96	1.06E-009	3.07	9.59E-0010	3.08	

Then we define the left and right fluxes as:

$$\hat{f}_{j+\frac{1}{2}}^l = F(U_{h,j+\frac{1}{2}}^{*,-}, U_{h,j+\frac{1}{2}}^{*,+}) + \begin{pmatrix} 0 \\ n_{h,j+\frac{1}{2}}^- - n_{h,j+\frac{1}{2}}^{*,-} \end{pmatrix} \quad (6.12)$$

$$\hat{f}_{j-\frac{1}{2}}^r = F(U_{h,j-\frac{1}{2}}^{*,-}, U_{h,j-\frac{1}{2}}^{*,+}) + \begin{pmatrix} 0 \\ n_{h,j-\frac{1}{2}}^+ - n_{h,j-\frac{1}{2}}^{*,+} \end{pmatrix} \quad (6.13)$$

3: We note that $(nu)_h = 0$ and n_h , satisfying $\frac{n_h}{(e^{\chi(c)})_h} = constant$, is the steady state solution of :

$$(nu^2 + n)_x = \frac{n}{(e^{\chi(c)})_h} \frac{d}{dx}(e^{\chi(c)})_h - \sigma nu.$$

With these three conditions, we can repeat the proof of Proposition 3.1 to show that our new schemes are indeed well balanced and high order accurate.

The limiter procedure is performed similarly as in Section 6.1. We refer to [33] for more details.

The following example is to test the fifth order accuracy for smooth solutions, for which we take the initial conditions as

$$n(x, 0) = 1 + 0.2 \cos(\pi x), \quad u(x, 0) = 0, \quad x \in [-1, 1]$$

with

$$c(x) = e^{-16x^2}, \quad \chi(c) = \log(1 + c), \quad \sigma = 0$$

with a periodic boundary condition. Since the exact solution is not known explicitly for this problem, we use the same fifth order WENO scheme with $N = 5120$ points to compute a reference solution and treat it as the exact solution when computing the numerical errors. Final time $t = 1.0s$ is used to avoid the development of shocks. The constant M is taken as 13 and the CFL number is 0.18 in the RKDG code. Table 7 contains the L^1 errors and numerical orders of accuracy. We can clearly see that the expected order accuracy is achieved for this example.

7 Concluding remarks

In this paper we have presented a new class of high order well balanced finite volume WENO and finite element discontinuous Galerkin schemes to several hyperbolic balance laws including the shallow water equations, the elastic wave equation, and the hyperbolic model for a chemosensitive movement. Our technique can also be applied to other application problems such as the nozzle flow problem and a two phase flow model [32], but we have not included them in this paper to save space. Traditional RKDG methods with a special treatment of the flux are proven to be well balanced for certain steady state solutions, and can maintain their original high order accuracy and essentially non-oscillatory property for general solutions. Finite volume WENO schemes can be modified due to similar ideas to obtain those properties. Extensive numerical examples are given to demonstrate the exactness property, accuracy, and non-oscillatory shock resolution of the proposed numerical method. The approach used in this paper is different from that used in [33]. Comparing with the well balanced schemes developed in [33], the well balanced RKDG schemes in this paper are simpler and involve less modification to the original RKDG methods, while the well balanced WENO finite volume schemes in this paper and that in [33] are comparable in computational cost.

References

- [1] E. Audusse, F. Bouchut, M.-O. Bristeau, R. Klein and B. Perthame, A fast and stable well-balanced scheme with hydrostatic reconstruction for shallow water flows, *SIAM J. Sci. Comput.*, 25 (2004), 2050-2065.
- [2] D. S. Bale, R. J. LeVeque, S. Mitran and J. A. Rossmannith, A wave propagation method for conservation laws and balance laws with spatially varying flux functions, *SIAM J. Sci. Comput.*, 24 (2002), 955-978.
- [3] D. S. Balsara and C.-W. Shu, Monotonicity preserving weighted essentially non-oscillatory schemes with increasingly high order of accuracy, *J. Comput. Phys.*, 160 (2000), 405-452.
- [4] A. Bermudez and M. E. Vazquez, Upwind methods for hyperbolic conservation laws with source terms, *Comput. Fluids*, 23 (1994), 1049-1071.
- [5] B. Cockburn, Discontinuous Galerkin methods for convection-dominated problems, in: T. J. Barth and H. Deconinck (Eds.), *High-Order Methods for Computational Physics*, Lecture Notes in Computational Science and Engineering, vol. 9, Springer, 1999, pp. 69-224.
- [6] B. Cockburn, S. Hou and C.-W. Shu, The Runge-Kutta local projection discontinuous Galerkin finite element method for conservation laws IV: the multidimensional case, *Math. Comput.*, 54 (1990), 545-581.
- [7] B. Cockburn, S.-Y. Lin and C.-W. Shu, TVB Runge-Kutta local projection discontinuous Galerkin finite element method for conservation laws III: one dimensional systems, *J. Comput. Phys.*, 84 (1989), 90-113.
- [8] B. Cockburn and C.-W. Shu, TVB Runge-Kutta local projection discontinuous Galerkin finite element method for conservation laws II: general framework, *Math. Comput.*, 52 (1989), 411-435.
- [9] B. Cockburn and C.-W. Shu, The Runge-Kutta discontinuous Galerkin method for conservation laws V: multidimensional systems, *J. Comput. Phys.*, 141 (1998), 199-224.
- [10] B. Cockburn and C.-W. Shu, Runge-Kutta discontinuous Galerkin methods for convection-dominated problems, *J. Sci. Comput.*, 16 (2001), 173-261.

- [11] F. Filbet and C.-W. Shu, Approximation of hyperbolic models for chemosensitive movement, *SIAM J. Sci. Comput.*, in press.
- [12] N. Goutal and F. Maurel, Proceedings of the Second Workshop on Dam-Break Wave Simulation, Technical Report HE-43/97/016/A, Electricité de France, Département Laboratoire National d'Hydraulique, Groupe Hydraulique Fluviale, 1997.
- [13] A. Harten, B. Engquist, S. Osher and S. Chakravathy, Uniformly high order accurate essentially non-oscillatory schemes, III, *J. Comput. Phys.*, 71 (1987), 231-303.
- [14] T. Hillen, Hyperbolic models for chemosensitive movement, *Math. Models Methods Appl. Sci.*, 12 (2002), 1007-1034.
- [15] C. Hu and C.-W. Shu, Weighted essentially non-oscillatory schemes on triangular meshes, *J. Comput. Phys.*, 150 (1999), 97-127.
- [16] G. Jiang and C.-W. Shu, Efficient implementation of weighted ENO schemes, *J. Comput. Phys.*, 126 (1996), 202-228.
- [17] S. Jin, A steady state capturing method for hyperbolic systems with geometrical source terms, *Math. Model. Numer. Anal.*, 35 (2001), 631-646.
- [18] A. Kurganov and D. Levy, Central-upwind schemes for the Saint-Venant system, *Math. Model. Numer. Anal.*, 36 (2002), 397-425.
- [19] R. J. LeVeque, Balancing source terms and flux gradients on high-resolution Godunov methods: the quasi-steady wave-propagation algorithm, *J. Comput. Phys.*, 146 (1998), 346-365.
- [20] X.-D. Liu, S. Osher and T. Chan, Weighted essentially nonoscillatory schemes, *J. Comput. Phys.*, 115 (1994), 200-212.
- [21] S. Noelle, N. Pankratz, G. Puppo and J. R. Natvig, Well-balanced finite volume schemes of arbitrary order of accuracy for shallow water flows, *J. Comput. Phys.*, in press.
- [22] G. Russo, Central schemes for balance laws, Proceedings of the VIII International Conference on Nonlinear Hyperbolic Problems, Magdeburg, 2000, pp. 821-929.
- [23] J. Shi, C. Hu and C.-W. Shu, A technique of treating negative weights in WENO schemes, *J. Comput. Phys.*, 175 (2002), 108-127.
- [24] C.-W. Shu, TVB uniformly high-order schemes for conservation laws, *Math. Comput.*, 49 (1987), 105-121.
- [25] C.-W. Shu, Essentially non-oscillatory and weighted essentially non-oscillatory schemes for hyperbolic conservation laws, in: A. Quarteroni (Ed.), *Advanced Numerical Approximation of Nonlinear Hyperbolic Equations*, Lecture Notes in Mathematics, vol. 1697, Springer, 1998, pp. 325-432.
- [26] C.-W. Shu and S. Osher, Efficient implementation of essentially non-oscillatory shock-capturing schemes, *J. Comput. Phys.*, 77 (1988), 439-471.
- [27] C.-W. Shu and S. Osher, Efficient implementation of essentially non-oscillatory shock-capturing schemes, II, *J. Comput. Phys.*, 83 (1989), 32-78.
- [28] M. E. Vazquez-Cendon, Improved treatment of source terms in upwind schemes for the shallow water equations in channels with irregular geometry, *J. Comput. Phys.*, 148 (1999), 497-526.
- [29] S. Vukovic and L. Sopta, ENO and WENO schemes with the exact conservation property for one-dimensional shallow water equations, *J. Comput. Phys.*, 179 (2002), 593-621.
- [30] S. Vukovic, N. Crnjacic-Zic and L. Sopta, WENO schemes for balance laws with spatially varying flux, *J. Comput. Phys.*, 199 (2004), 87-109.
- [31] Y. Xing and C.-W. Shu, High order finite difference WENO schemes with the exact conservation property for the shallow water equations, *J. Comput. Phys.*, 208 (2005), 206-227.
- [32] Y. Xing and C.-W. Shu, High order well-balanced finite difference WENO schemes for a class of hyperbolic systems with source terms, *J. Sci. Comput.*, in press.
- [33] Y. Xing and C.-W. Shu, High order well-balanced finite volume WENO schemes and discontinuous

- Galerkin methods for a class of hyperbolic systems with source terms, *J. Comput. Phys.*, in press.
- [34] J. G. Zhou, D. M. Causon, C. G. Mingham and D. M. Ingram, The surface gradient method for the treatment of source terms in the shallow-water equations, *J. Comput. Phys.*, 168 (2001), 1-25.
- [35] T. Zhou, Y. Li and C.-W. Shu, Numerical comparison of WENO finite volume and Runge-Kutta discontinuous Galerkin methods, *J. Sci. Comput.*, 16 (2001), 145-171.